

---

Theses and Dissertations

---

Fall 2015

# Validation of CFD-MBD FSI for high-fidelity simulations of full-scale WAM-V sea-trials with suspended payload

Michael Anthony Conger  
*University of Iowa*

Copyright 2015 Michael Anthony Conger

This thesis is available at Iowa Research Online: <http://ir.uiowa.edu/etd/1960>

---

## Recommended Citation

Conger, Michael Anthony. "Validation of CFD-MBD FSI for high-fidelity simulations of full-scale WAM-V sea-trials with suspended payload." MS (Master of Science) thesis, University of Iowa, 2015.  
<http://ir.uiowa.edu/etd/1960>.

---

Follow this and additional works at: <http://ir.uiowa.edu/etd>

 Part of the [Mechanical Engineering Commons](#)

VALIDATION OF CFD-MBD FSI FOR HIGH-FIDELITY SIMULATIONS  
OF FULL-SCALE WAM-V SEA-TRIALS WITH SUSPENDED PAYLOAD

by

Michael Anthony Conger

A thesis submitted in partial fulfillment  
of the requirements for the Master of Science  
degree in Mechanical Engineering in the  
Graduate College of  
The University of Iowa

December 2015

Thesis Supervisors: Professor Frederick Stern  
Research Scientist/Adjunct Professor Maysam  
Mousaviraad

Graduate College  
The University of Iowa  
Iowa City, Iowa

CERTIFICATE OF APPROVAL

---

MASTER'S THESIS

---

This is to certify that the Master's thesis of

Michael Anthony Conger

has been approved by the Examining Committee for  
the thesis requirement for the Master of Science degree  
in Mechanical Engineering at the December 2015 graduation.

Thesis Committee:

---

Frederick Stern, Thesis Supervisor

---

Maysam Mousaviraad, Thesis Supervisor

---

H.S. Udaykumar

This thesis is dedicated to my dearest Jessica and our amazing daughter Sophia, for their unconditional love and support. I also dedicate this thesis to my mother, for her continual support of my studies.

## ACKNOWLEDGEMENTS

I would like to sincerely thank Professor Frederick Stern, my research advisor, for allowing me the opportunity to carry out research under his guidance, and for providing support and encouragement. I would also like to sincerely thank Dr. Maysam Mousaviraad, my research co-advisor, without your support, encouragement, and guidance, I would never have been able to complete this work. I am grateful for both of their contributions to my research and education.

I would like to thank the research faculty and support faculty at IIHR-Hydroscience & Engineering for their support and for providing a wonderful research environment.

I would like to thank our collaborators at Virginia Polytechnic Institute and State University, Andrew Peterson and Mehdi Ahmadian, for their contributions.

This research was conducted under the sponsorship of Office of Naval Research under Grants 000141-21-05-6-0 (University of Iowa) and 000140-91-06-1-5 (Virginia Tech University) administered by Ms. Kelly Cooper. Partial sponsorship of this research was granted by Naval Engineering Education Consortium (NEEC) under the administration of Prof. Steven Ceccio.

This research was supported in part through computational resources provided by The University of Iowa, Iowa City, Iowa.

## ABSTRACT

High-fidelity CFD-MBD FSI (Computational Fluid Dynamics - Multi Body Dynamics Fluid-Structure Interaction) code development and validation by full-scale experiments is presented, for a novel hull form, WAM-V (Wave Adaptive Modular Vessel). FSI validation experiments include cylinder drop with suspended mass and 33 ft WAM-V sea-trials. Calm water and single-wave sea-trials were with the original suspension, while the rough-water testing was with a second generation suspension. CFDShip-Iowa is used as CFD solver, and is coupled to Matlab Simulink MBD models for cylinder drop and second generation WAM-V suspension. For 1DOF cylinder drop, CFD verification and validation (V&V) studies are carried out including grid and time-step convergence. CFD-MBD results for 2DOF cylinder drop show that 2-way coupling is required to capture coupled physics. Overall, 2-way results are validated with an overall average error value of  $E=5.6\%DR$  for 2DOF cylinder drop. For WAM-V in calm water, CFD-MBD 2-way results for relative pod angle are validated with  $E=14.2\%DR$ . For single-wave, CFD-MBD results show that 2-way coupling significantly improves the prediction of the peak amplitude in pontoon motions, while the trough amplitudes in suspension motions are under-predicted. The current CFD-MBD 2-way results for single-wave are validated with  $E=17\%DR$ . For rough-water, simulations are carried out in regular head waves representative of the irregular seas. CFD-MBD 2-way results are validation with  $E=23\%D$  for statistical values and the Fourier analysis results, which is reasonable given the differences between simulation waves and experiments.

## **PUBLIC ABSTRACT**

A wave adaptive modular vessel (WAM-V) is studied and computer models, simulating the coupled suspension dynamics and pontoon hydrodynamics, are developed and validated against sea-trial data. A WAM-V is a class of suspension sea-going vessel that conforms to the surface of waves through flexible catamaran style pontoons, a suspension system that independently articulates, and hinged engine pods.

Simulations are performed and validated independently, simulating the hydrodynamics (water-pontoon interaction), and simulating the suspension dynamics, and coupled, where the dynamic motions of the suspension are accounted for in the hydrodynamic simulation. This coupling method is referred to as fluid structure interaction, and is the objective of this thesis.

Experiments are used to validate independent and coupled simulations for both a full scale WAM-V and a simple pontoon-sprung-mass system. The pontoon-sprung-mass experiments are used to initially validate hydrodynamic modeling, suspension modeling, and simulation coupling methodology. The WAM-V experiments are used to validate suspension system modeling and coupled simulations in calm water, over a single stern wake of a freighter ship, and in rough waters.

The results from the independent simulations for the pontoon-sprung-mass experiments and the WAM-V show good agreement with experimental data. The results from the coupled simulations compared to the independent simulations show that it is necessary in cases with complex coupled physics to have a coupled simulation to capture important phenomena that is missed in independent simulations.

# TABLE OF CONTENTS

LIST OF TABLES .....	viii
LIST OF FIGURES .....	ix
CHAPTER 1 INTRODUCTION.....	1
CHAPTER 2 PONTOON-SUSPENSION FSI VALIDATION EXPERIMENTS .....	5
2.1 Cylinder Drop Experiments .....	5
2.2 WAM-V Experiments .....	11
2.2.1 Shaker Rig.....	13
2.2.2 Calm Water .....	15
2.2.3 Single-Wave.....	16
2.2.4 Rough Water .....	22
CHAPTER 3 COMPUTATIONAL METHODS .....	25
3.1 Overview of CFDShip-Iowa Version 4.5 .....	25
3.1.1 Two-Body Dynamics for Hinged Engine Pod.....	25
3.1.2 LS-IBM for Pontoon-Pod Gap.....	27
3.1.3 Jet Force Model for Validation against Free-Running Experiments .....	28
3.2 Simulink Multi-Body Dynamics.....	29
3.3 CFD-MBD Coupling .....	30
CHAPTER 4 SIMULATION CONDITIONS AND VALIDATION APPROACH.....	33
4.1 Cylinder Drop .....	33
4.1.1 Drop Height Determination .....	33
4.1.2 V&V Grid and Time-step .....	34
4.1.3 Friction Studies .....	34
4.1.4 Validation Approach.....	35
4.2 Shaker Rig MBD Validation.....	36
4.3 WAM-V Sea-Trials.....	36
4.3.1 Calm Water Simulation.....	37
4.3.1.1 Hydrostatic Setup.....	37
4.3.1.2 Validation Approach.....	37
4.3.2 Single-Wave Simulation .....	38
4.3.2.1 Input Waves for Validation Simulation .....	38
4.3.2.2 Validation Approach.....	39
4.3.3 Rough Water Simulation.....	39
4.3.3.1 Input Waves for Validation Simulation .....	39
4.3.3.2 Validation Approach.....	40



CHAPTER 5	CFD V&V FOR 1-DOF CYLINDER DROP .....	41
	5.1 Grid and Time-step Verification Results .....	41
	5.2 Friction.....	42
	5.3 Validation Results.....	43
CHAPTER 6	MBD VALIDATION RESULTS .....	47
	6.1 WAM-V Un-Coupled MBD Validation against Shaker Rig Laboratory Experiment .....	47
	6.2 EFD-MBD for Un-Coupled MBD Validation against On-Water Data .....	47
	6.2.1 Cylinder Drop .....	47
	6.2.2 WAM-V Single-Wave .....	50
CHAPTER 7	CFD-MBD FSI VALIDATION RESULTS.....	52
	7.1 2DoF Cylinder Drop .....	52
	7.2 WAM-V Calm Water.....	57
	7.3 WAM-V Single-Wave .....	61
	7.4 WAM-V Rough Water.....	65
CHAPTER 8	CONCLUSION AND FUTURE WORK.....	70
REFERENCES	.....	73

## LIST OF TABLES

Table 2-1 Experimental drop test configuration information for cylinder drop test rig [16].....	7
Table 2-2 Seven suspension phases of WAM-V travelling through single-wave event (figures from [16]).....	18
Table 2-3 Statistical results for rough-water testing.....	24
Table 3-1 - Input variables for MBD code.....	30
Table 4-1 Corrected drop heights for CFD grid correction .....	34
Table 5-1 CFD verification and validation (V&V) results for 1DoF cylinder drop .....	41
Table 5-2 Linear friction coefficient studies for 1DoF cylinder drop $h=0.26[m]$ .....	42
Table 5-3 1DoF cylinder drop validation results .....	44
Table 7-1 2DoF Cylinder drop validation results .....	54
Table 7-2 WAM-V calm water validation results.....	58
Table 7-3 WAM-V single-wave encounter validation results .....	62
Table 7-4 WAM-V rough-water sea-trials and CFD-MBD validation simulations in regular waves representation of the irregular seas.....	66

## LIST OF FIGURES

Figure 2-1 Cylinder drop test rig (lef) and schematic of the components (right) [16] .....	7
Figure 2-2 Cylinder drop experimental data collection instrument schematic [16] .....	7
Figure 2-3 EFD data for 1DoF cylinder drop tests (EFD data from [16]).....	8
Figure 2-4 EFD data for 2DoF cylinder drop test h=0.20 m (EFD data from [16]).....	9
Figure 2-5 EFD data for 2DoF cylinder drop test h=0.26 m (EFD data from [16]).....	10
Figure 2-6 33 ft WAM-V in calm water (top left) and in waves (top right) and component diagram (bottom) (annotated from [16]).....	12
Figure 2-7 Schematic of instrumentation used for data collection on WAM-V sea-trials [16] .....	12
Figure 2-8 2-post shaker rig experiment schematic [16] .....	13
Figure 2-9 Pontoon cradle and rear post of 2-post shaker rig [16] .....	14
Figure 2-10 2-post shaker rig experimental setup [16].....	14
Figure 2-11 WAM-V engine pod rotation data at incremental throttle positions [16] ....	15
Figure 2-12 EFD pontoon motion data for WAM-V single-wave test (EFD data from [16]) .....	19
Figure 2-13 EFD engine pod and suspension motion data for WAM-V single-wave test (EFD data from [16]).....	20
Figure 2-14 Suspension displacement for both port and starboard sides broken down by relevant phases [16] .....	21
Figure 2-15 Pontoon acceleration measured at the front of the WAM-V (EFD data from [16]) .....	21
Figure 2-16 Sea-trial trajectory for WAM-V rough -water testing and the direction of dominant waves .....	23
Figure 2-17 Comparison of time histories and running RMS for EFD and CFD accelerations at the front and rear posts .....	23
Figure 2-18 FFT results for EFD accelerations at the front and rear posts.....	24
Figure 3-1 Block diagram for two-body dynamics model for hinged engine pod simulations [6] .....	27

Figure 3-2 Level-set immersed boundary method (LS-IBM) implemented to treat the flow inside the gap .....	28
Figure 3-3 WAM-V MBD model: Input motions (left) and total degrees of freedom (right) .....	30
Figure 3-4 Block diagrams for CFD-MBD one-way (left) and two-way (right) coupling.....	32
Figure 4-1 Snapshot of grid and free-surface during a 1DoF cylinder drop simulation.....	33
Figure 4-2 Overset grid (left) and half-domain design (right) for WAM-V simulations .....	37
Figure 4-3 Procedure to design an estimate wave group as input to CFDSHIP-IOWA for the single-wave validation simulation.....	39
Figure 5-1 Linear friction studies for 1DoF cylinder drop $h=0.26[m]$ (EFD data from [16]) .....	43
Figure 5-2 Validation results for 1DoF cylinder drop $h=0.20[m]$ (EFD data from [16]) .....	45
Figure 5-3 Validation results for 1DoF cylinder drop $h=0.26[m]$ (EFD data from [16]) .....	46
Figure 6-1 Validation of MBD code via 2-post shaker rig experiment (data from [16]).....	47
Figure 6-2 EFD-MBD validation results for 2DoF cylinder drop at $h=0.20$ m and $h=0.26$ m (EFD data from [16]).....	49
Figure 6-3 EFD-MBD validation results for single-wave simulation (EFD data from [16]) .....	51
Figure 7-1 Validation results for 2DoF cylinder drop $h=0.20[m]$ .....	55
Figure 7-2 Validation results for 2DoF cylinder drop $h=0.26[m]$ .....	56
Figure 7-3 WAM-V calm water results .....	59
Figure 7-4 Free-surface and WAM-V motions for calm water simulations.....	60
Figure 7-5 WAM-V single-wave simulation results.....	63
Figure 7-6 Snapshots of experimental videos and CFD-MBD simulations during single-wave event .....	64

Figure 7-7 WAM-V rough-water validation results against acceleration data ..... 67

Figure 7-8 Comparison of CFD-MBD 1-way and 2-way simulations in regular waves..... 68

Figure 7-9 Free-surface and WAM-V motions for simulations in regular waves ..... 69

## CHAPTER 1 INTRODUCTION

Most of the multi-body dynamics (MBD) modeling studies in the literature are carried out for simulations of automobile suspension systems. Road profiles are imposed as base excitations utilizing quarter-vehicle (e.g. [9, 18]), half-vehicle (e.g. [4, 19]), or full-vehicle (e.g. [5, 14]) models. Commercial software have been used to develop MBD models, such as MATLAB Simulink in [18]. Only limited studies have coupled MBD with other physics-based models. For example, Nassif & Liu [13] coupled MBD for car suspension with bridge dynamic structural model, and studied the bridge-road-vehicle interaction problem caused by multiple moving trucks on a bridge with random road roughness.

Computational fluid dynamics (CFD) solvers with rigid motion capabilities are coupled with cable dynamics models for MBD motions of moored offshore platforms (e.g. [20, 10, and 17]). Motions and point forces are exchanged between the two solvers to compute the fluid-structure interactions (FSI). The flow solvers in the above referenced studies are based on potential flow or smoothed particle hydrodynamics (SPH) methods. Studies with CFD-MBD coupling for simulations of vehicles with suspension systems are not included in the literature.

The Wave Adaptive Modular Vessel (WAM-V) is an ultra-light flexible catamaran that conforms to the surface of the water through an articulation system that allows the hulls to move semi-independently, a suspension system for the payload module, hinged engine pods, and soft inflatable pontoon hulls [3].

Experimental fluid dynamics (EFD) studies for WAM-V include manned and unmanned demonstrative trials, as well as limited laboratory and on-sea data collections for validation studies. Hull motions are recorded during sea-trials of the 100 ft ‘Proteus’

including calm water propulsion and seakeeping [1]. Towing tank experiments in calm water are carried out for a 12 ft WAM-V model where resistance, sinkage and trim are measured at 11 Froude numbers ranging from 0.17 to 1.12 [7]. Sea-trials are conducted for a 12 ft WAM-V unmanned surface vessel (USV) by Peterson & Ahmadian [15], where displacements and accelerations are measured both for hulls and suspension in sea-state 2 conditions at different speeds and wave headings.

FSI experiments are carried out by Peterson [16], which is used in the present study as validation data. The experiments include a two-degree-of-freedom (2DOF) cylinder drop with suspended mass, as well as WAM-V sea-trials. Cylinder drop experiments are carried out as preliminary step with fewer degrees of freedom conducted in a controlled and repeatable environment. 1DOF experiments are also carried out with suspension locked out. WAM-V sea-trials are with a 33 ft manned vessel with waterjet propulsion. The measurement equipment includes accelerometers and potentiometers on pontoon and suspension, as well as GPS and video cameras. The available data are for calm water, a single-wave testing over the stern wake of a large freighter ship, and a rough-water testing.

A system-based (SB) model is developed for cylinder drop and validated against the 1DOF experiments [16]. The model simulates the hydrodynamic interactions as a spring-mass-damper system with the addition of a variable added mass dependent on the instantaneous immersion of the cylinder. Friction in the guide rails is modeled using a bi-linear damping.

CFD models for WAM-V captive simulations are developed and implemented into CFDShip-Iowa, an unsteady Reynolds averaged Navier-Stokes (URANS) flow solver [12]. The WAM-V models include two-body dynamics for hinged engine pods and immersed

boundary treatment for the gap between pontoons and pods. Captive validation studies are carried out against the model-scale calm water towing tank data by Helsel et al. [7]. Only CFD modeling is included, where pontoon hull and suspension are assumed rigid. Comparison error for resistance, sinkage, and trim, averaged over 10 Froude numbers (ranging from  $Fr=0.17$  to  $1.12$ ), was  $E=5.7\%D$ .

A jet-force model is implemented into CFDSHIP-IOWA for free-running CFD capabilities and validation studies against full-scale (33 ft) WAM-V sea-trials in calm water and rough-water are carried out [2]. For rough-water, CFD results in regular waves, representative of the irregular seas, are validated against expected values (EV) and standard deviations (SD) of motion and acceleration data.

MBD models are developed, using Matlab Simulink, both for 2DOF cylinder drop [16] and WAM-V [6, 16]. The MBD model for WAM-V is validated by a shaker rig experiment enforcing pontoon motions as base excitation [2]. The enforced motions are based on the CFD results in regular head waves representative of the rough-water sea-trial conditions.

SB-MBD coupling is carried out for 2DOF cylinder drop [16], and the results are evaluated and included in the present paper for comparison. Preliminary CFD-MBD studies are carried out for cylinder drop [2]. The results are improved, by re-evaluating the drop heights, and presented in the current paper.

The objective of present collaborative research is CFD-MBD FSI code development for WAM-V and validation by full-scale sea-trial experiments.

The approach is completing the cylinder drop studies prior to WAM-V, including CFD verification and validation (V&V) studies for 1DOF and detailed CFD-MBD validation



studies of the pontoon and sprung mass for 2DOF. Building on cylinder drop studies, CFDShip-Iowa code is coupled to the Matlab Simulink MBD model for WAM-V. The flexible pontoons are modeled as rigid body. In one-way coupling, suspension is affected by pontoon motions but not the other way around. Two-way coupling includes non-linear inner iterations to converge on flow field, pontoon motions, pod motions, suspension motions, and jet-force. Calm water results are validated with the relative pod angles. For single-wave simulations, incoming waves are generated using Fourier reconstruction of the visually estimated waves during sea-trials adjusted by the relative amplitudes and periods of the measured pontoon motions. The CFD-MBD results in regular waves, representative of the irregular rough-water conditions, are compared against the data for EV, SD, and dominant frequencies and amplitudes of accelerations at the front and rear accelerometer posts on the starboard and port pontoons, and at the suspension accelerometer post.

## CHAPTER 2 PONTOON-SUSPENSION FSI VALIDATION EXPERIMENTS

### 2.1 Cylinder Drop Experiments

The test rig and a schematic of the test design and its major components are shown in Figure 2-1. The suspension system consists of two linear coil springs located coaxially with the linear guide rails. The pontoon is 8 inches in diameter and 8 feet in length and is made of rigid polycarbonate, unlike the soft inflatable WAM-V pontoons. The degrees of freedom are provided by linear slide bearings in the sprung mass and pontoon that ride on the linear guide rails. Although significant care was taken to minimize the friction in the guide rails, there is still a small amount of friction in the system. A lock-out mechanism is used for 1DoF tests that locks the connection between the payload and the pontoon. 1DoF and 2DoF tests were conducted with different mass configurations and drop heights. Present studies focus on the two maximum heights,  $h=0.20$  m and  $0.26$  m, with maximum un-sprung and sprung masses of  $10.6$  kg and  $15.9$  kg, respectively. Two drops were performed for each different configuration.

Various sensors are used, as shown in Figure 2-2, providing validation variables for displacements and accelerations of the pontoon and the payload structure. The suspended mass is equipped with a 10G and a 3G accelerometer and the pontoon is equipped with a 30G and a 10G accelerometer. String potentiometers are positioned to measure the relative displacement between the top plate of the testing rig and the sprung mass, and the sprung mass and the pontoon. The height above water, the distance from the bottom of the pontoon to the free-surface, is measured before release and then is measured using the two string potentiometers.

A battery of drop tests were carried out showing a nonlinearity in the recorded rebound height of the pontoon [16]. The nonlinearity was noticed at the second highest drop height, both with and without ballast, when the second highest drop rebounds higher than the highest drop. This is attributed to the spray directing outward at lower drop heights and inward at the highest drop height. It was recommended by Andrew Peterson at Virginia Tech, to simulate the two highest drop heights to capture the nonlinearity in the rebound height. Table 2-1 shows drop tests which were selected for analysis, including drop height, spring configuration, and the ballast configuration.

Cylinder drop experimental data is shown in Figure 2-3 to Figure 2-5. The pontoon and suspension displacement and accelerations are recorded from sensors while the pontoon velocity and suspension velocity is calculated through numerical differentiation of the pontoon displacement, employing a central differencing scheme. To eliminate high frequency noise in the velocities, a data smoothing method was applied to the velocity curves. The average motions of the two cylinder drops is calculated and shown with error bars on the pontoon and suspension displacement for both error in time, and error in displacement at the extrema. The displacement extrema error values are calculated by differencing the time and amplitude of extrema between the two drops.

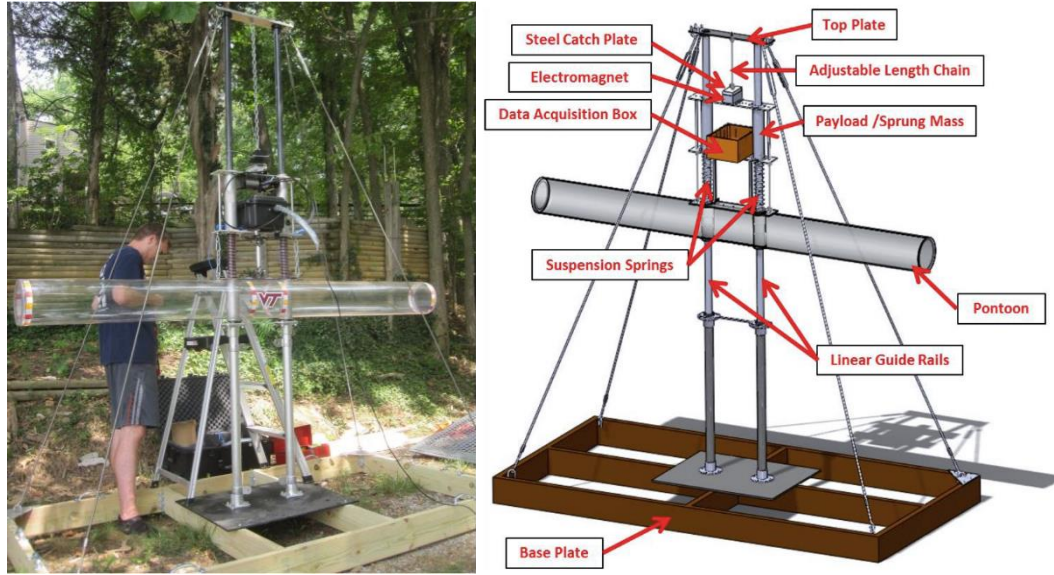


Figure 2-1 Cylinder drop test rig (left) and schematic of the components (right) [16]

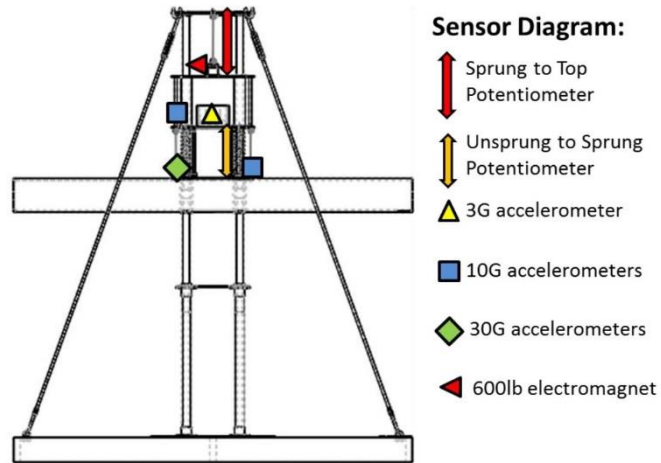


Figure 2-2 Cylinder drop experimental data collection instrument schematic [16]

Table 2-1 Experimental drop test configuration information for cylinder drop test rig [16]

Test #	Height above water [m]	Spring Configuration	Ballast Configuration Sprung / Unsprung [lbs]
9, 10	0.20	locked	5, 5
11, 12	0.26	locked	5, 5
21, 22	0.20	2 springs	5, 5
23, 24	0.26	2 springs	5, 5

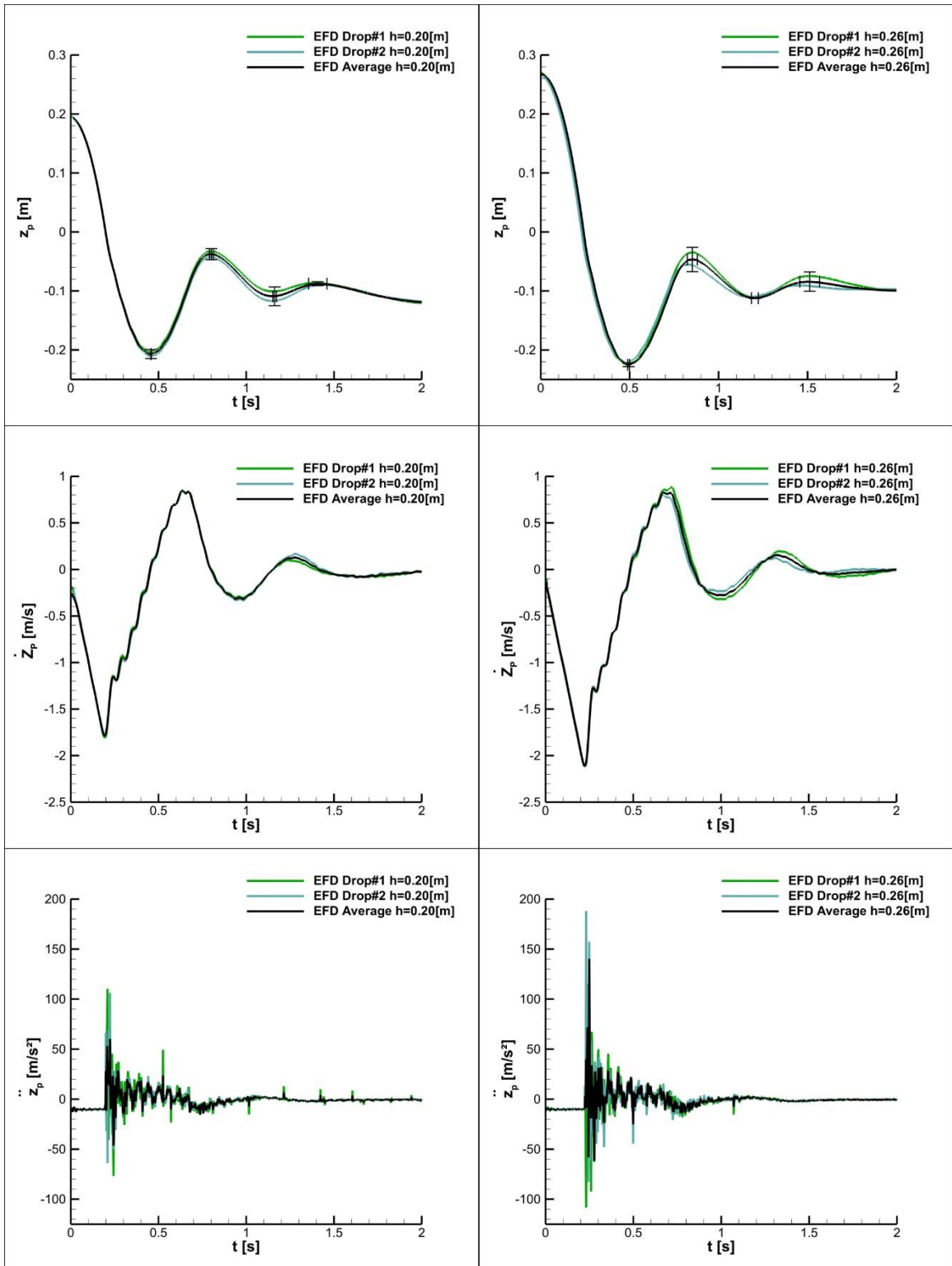


Figure 2-3 EFD data for 1DoF cylinder drop tests (EFD data from [16])

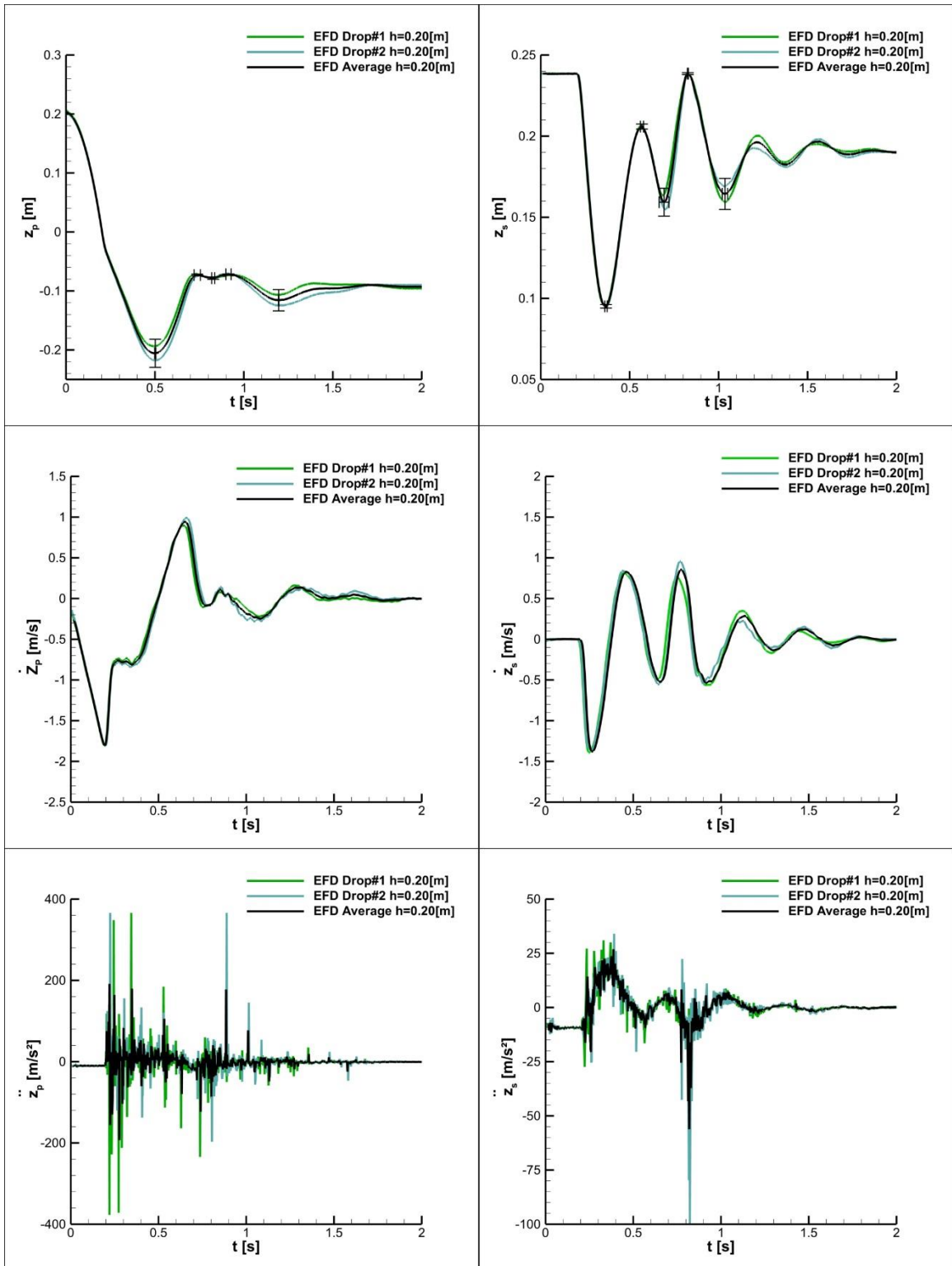


Figure 2-4 EFD data for 2DoF cylinder drop test  $h=0.20$  m (EFD data from [16])

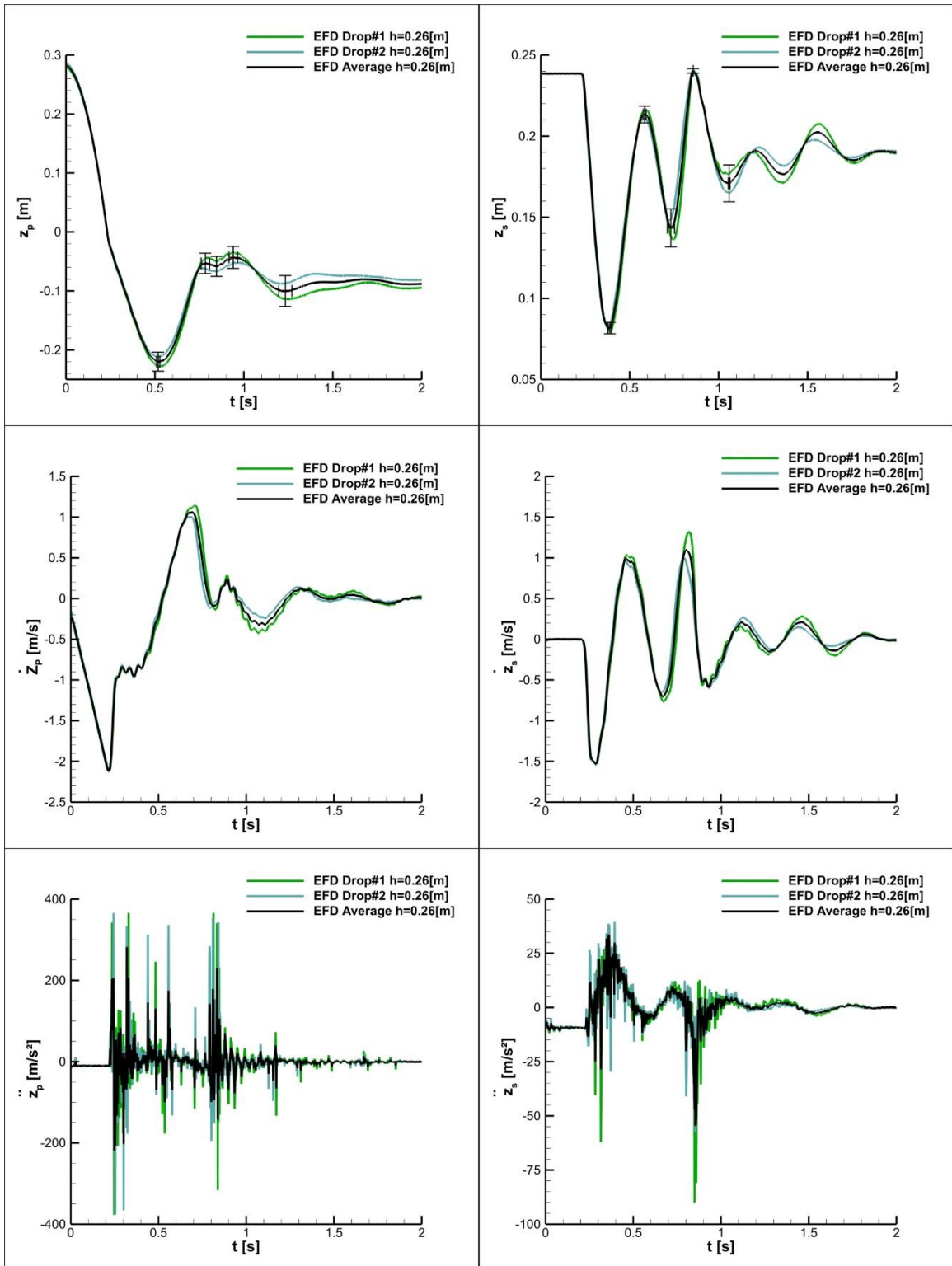


Figure 2-5 EFD data for 2DoF cylinder drop test  $h=0.26$  m (EFD data from [16])

## 2.2 WAM-V Experiments

WAM-V data was collected from full-scale sea-trials performed on the 33 ft version of the vessel, as shown in Figure 2-5. The components of the WAM-V hull and suspension and articulation systems are also shown in Figure 2-5. Calm water and single-wave testing were conducted with the original suspension design, while an improved second generation suspension was designed and used for rough-water testing [16]. The original suspension design uses an air spring and two viscous dampers, whereas the second generation replaces the air spring and dampers with a single coil-over spring and damper unit.

Validation variables include only engine pod angle relative to pontoon for calm water testing, while for testing in waves, a variety of sensor measurements are provided, as shown in Figure 2-6. Accelerometers, rotary and string potentiometers, GPS, and video recording data were collected. Accelerometers record accelerations at each of the four posts on pontoon (front and rear, right and left), at the end of the engine pod, and at the front of the payload (vertical and longitudinal). Rotary potentiometers were used to record the rotational travel of the front suspension; located on the front posts, and the engine pod rotational travel. The relative engine pods are limited in rotation from to -5 degrees (upward) to +15 degrees (downward). For upward rotations, the engine pods move freely to -1 degrees, after which compression bumpers are engaged. The GPS is located in the front of the payload.



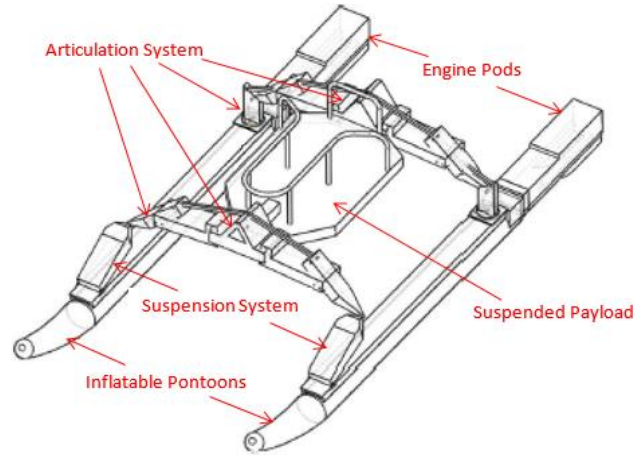


Figure 2-6 33 ft WAM-V in calm water (top left) and in waves (top right) and component diagram (bottom) (annotated from [16])

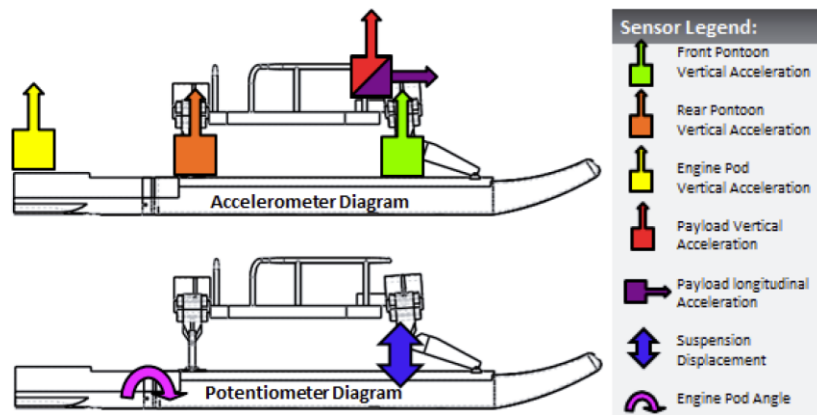


Figure 2-7 Schematic of instrumentation used for data collection on WAM-V sea-trials [16]

### 2.2.1 Shaker Rig

A 2-post shaker rig experiment (Figure 2-7) was designed and implemented by Peterson [16] to evaluate suspension dynamics of the 33 ft WAM-V. The two front posts are excited by hydraulic actuators with a total stroke of 6 inches ( $\pm 3$  inches), while two rear posts are used to support the rear of the WAM-V. The front posts are excitable by a continuous signal input to a hydraulic controller. The pontoons are too flexible to be held locally, therefore a semi-rigid rigid cradle (Figure 2-8) is used to connect the front and rear posts on either side. This semi-rigid cradle has been shown to eliminate some of the dynamics noticed from the pontoons caused by the addition of the bending stiffness of the cradle. The 2-post shaker rig experimental setup with the WAM-V attached, is shown in Figure 2-10.

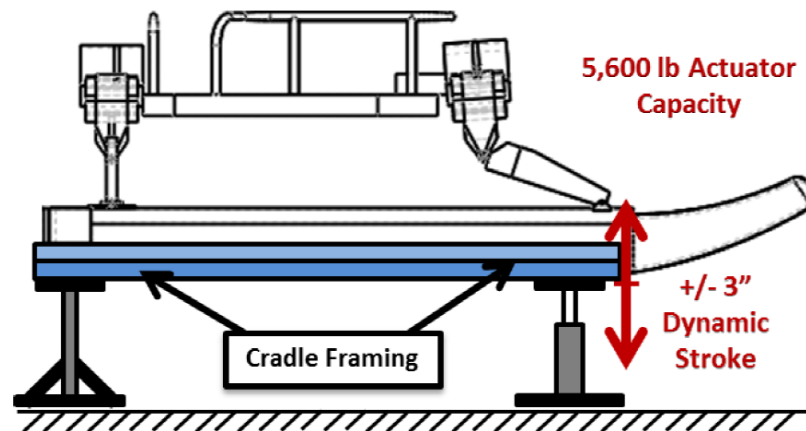


Figure 2-8 2-post shaker rig experiment schematic [16]

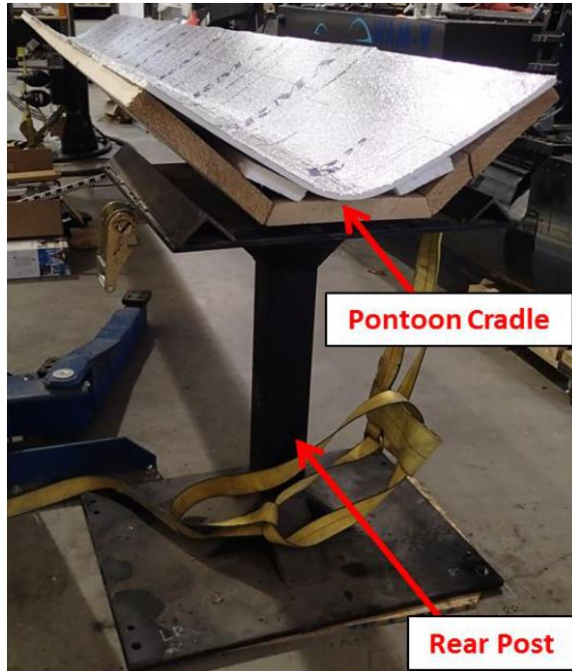


Figure 2-9 Pontoon cradle and rear post of 2-post shaker rig [16]



Figure 2-10 2-post shaker rig experimental setup [16]

### 2.2.2 Calm Water

Calm water testing was conducted with the 33 ft WAM-V with the original suspension system. The testing included running the WAM-V in calm waters at idle speed and then increasing the throttle percentage incrementally by 25 percent, corresponding to different constant forward speeds, waiting for the WAM-V response to become steady and then adjusting throttle to next increment. The WAM-V steady state response characteristics at different Froude numbers is measured, using the GPS data to calculate the vessel speed. Figure 2-11 shows the response of the WAM-V hinged engine pods to different forward speeds corresponding to the different throttle positions. The pod rotation uncertainty from port to starboard side, averaged over four Froude numbers, is 6.76%DR.

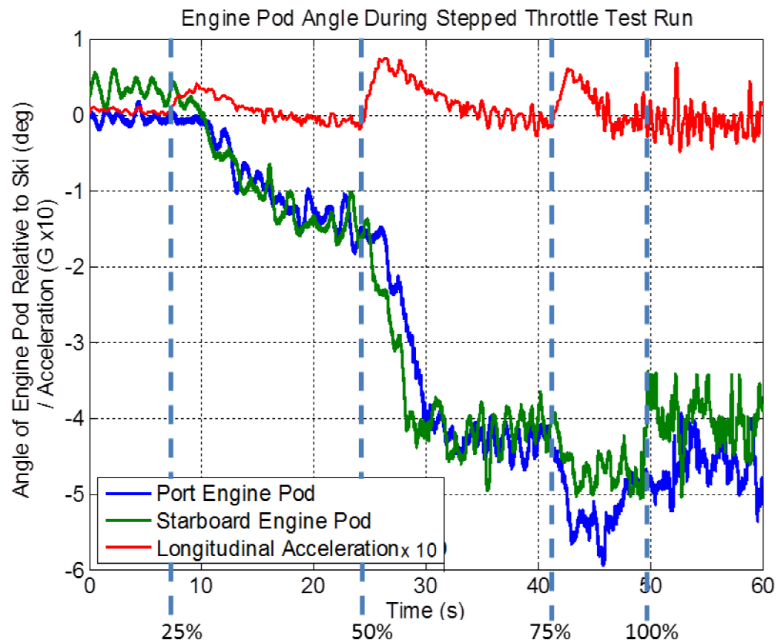


Figure 2-11 WAM-V engine pod rotation data at incremental throttle positions [16]

### 2.2.3 Single-Wave








The single-wave test was conducted by maneuvering the 33 ft WAM-V over the stern wake of a large freighter ship at a speed of 10 knots. The freighter ship produced an estimated 48 inch tall wave, with an estimated wave length approximately equal to the length of the WAM-V, estimated with video footage. Heading was set for a head sea condition relative to the freighter's wake. The wave was large enough to launch the WAM-V airborne during the test.

The WAM-V dynamics during the single-wave test is broke down by relevant phases [16] which are helpful in reproducing the wave computationally. The initial encounter has the WAM-V approaching the single-wave at 10 knots head sea. The WAM-V strikes the single wave in the loading phase causing the pontoons to deflect significantly and the suspension to compress to 85%. The WAM-V launches off of the single-wave during the unloading phase, where the suspension fully unloads hitting the limiting straps. The WAM-V then free-falls where the engine pods rotate downwards until hitting their limiting straps. The WAM-V hits the face of the next trailing wave, causing the suspension to compress to 90% and the engine pods rotate upwards to limiting stop. The WAM-V then unloads and oscillates in the following waves. The relevant phases of the WAM-V is shown graphically in Table 2-2.

Recorded data from single-wave test include accelerations at the front and rear of the pontoon for both sides, suspension displacement, and engine pod rotations. The non-measured kinematic motions, including pontoon velocity and displacement, suspension velocity and acceleration, and engine pod rotational velocity and rotational acceleration, are all found using numerical differentiation and/or integration of collected data. Front and

rear pontoon motions are shown in Figure 2-12 and suspension motions and engine pod motions are shown in Figure 2-13. The suspension displacement is broken down by relevant phases in Figure 2-14. Figure 2-15 shows a zoomed in view of the recorded acceleration at the front of the pontoon, indicating there is a small amount asymmetry in the experiment by the phase lag between port and starboard pontoon accelerations.

**Table 2-2 Seven suspension phases of WAM-V travelling through single-wave event (figures from [16])**

<p>Phase 1 – Initial Encounter</p>	 <p>Time = 0.00 sec</p>
<p>Phase 2 – Loading Phase</p>	 <p>Time = 0.79 sec</p>
<p>Phase 3 – Unloading Phase</p>	 <p>Time = 1.50 sec</p>
<p>Phase 4 – Free-Fall Phase</p>	 <p>Time = 1.74 sec</p>
<p>Phase 5 – Initial Impact</p>	 <p>Time = 1.84 sec</p>
<p>Phase 6 – Maximum Compression</p>	 <p>Time = 2.17 sec</p>
<p>Phase 7 – Secondary Oscillation</p>	 <p>Time = 2.94 sec</p>

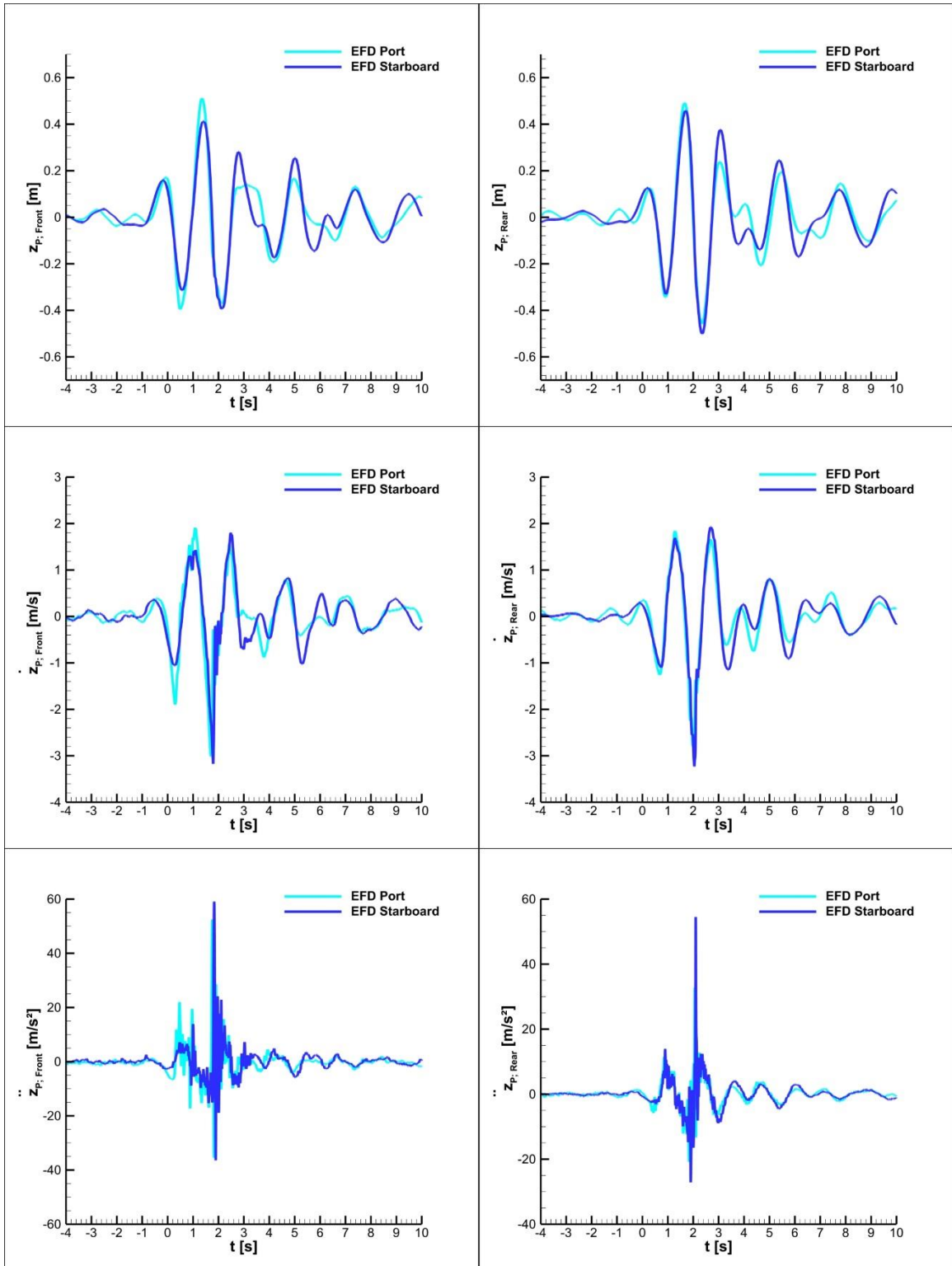


Figure 2-12 EFD pontoon motion data for WAM-V single-wave test (EFD data from [16])



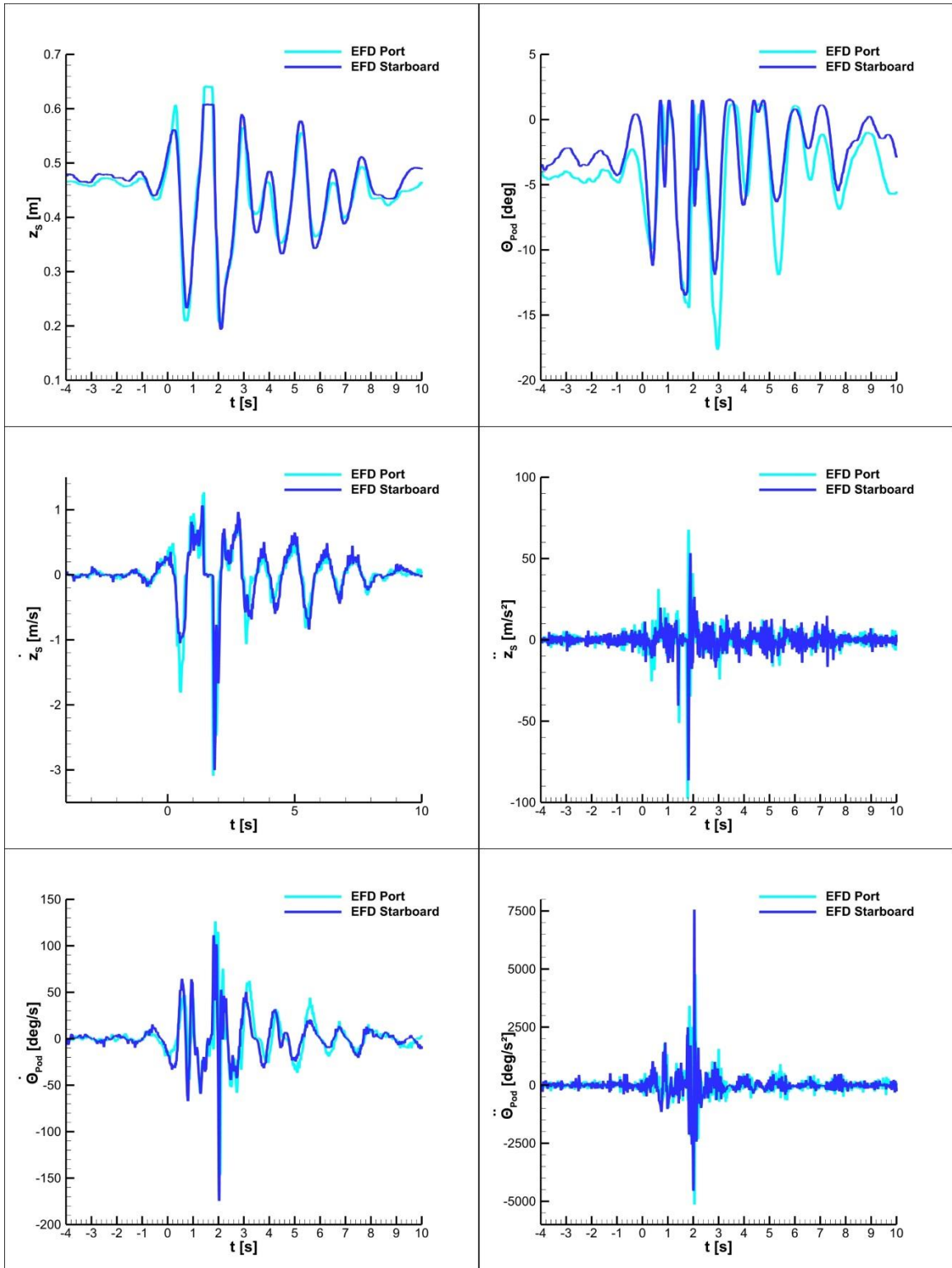
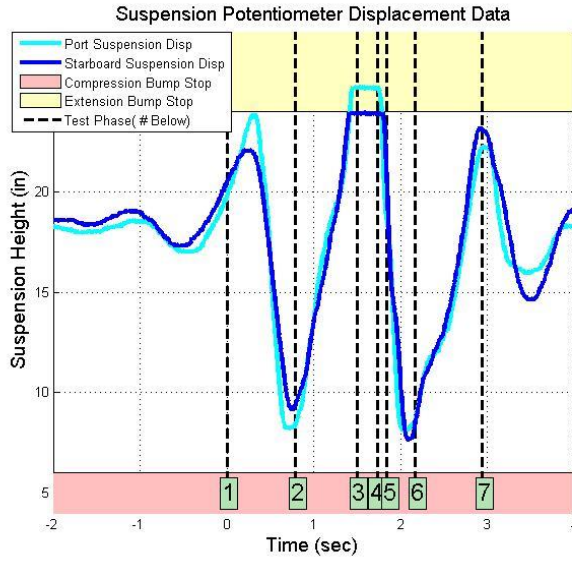
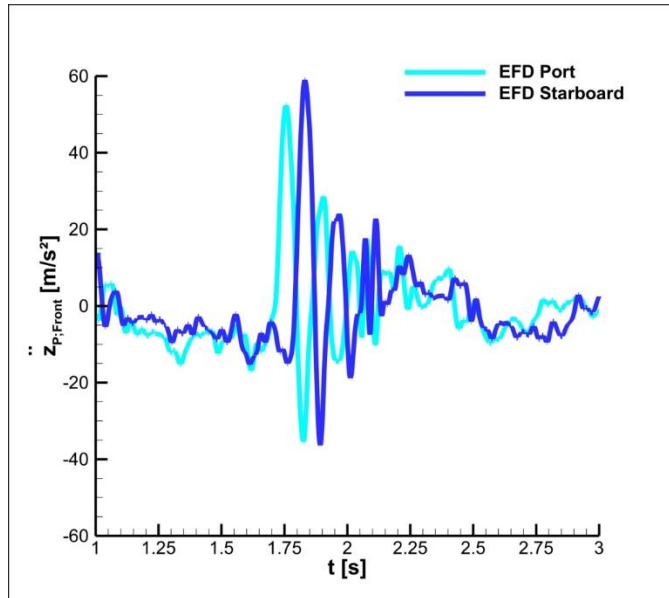


Figure 2-13 EFD engine pod and suspension motion data for WAM-V single-wave test (EFD data from [16])



**Figure 2-14 Suspension displacement for both port and starboard sides broken down by relevant phases [16]**



**Figure 2-15 Pontoon acceleration measured at the front of the WAM-V (EFD data from [16])**

#### 2.2.4 Rough Water

Rough-water testing was conducted at a speed of 10 knots at the Naval Base in Norfolk, VA. The trajectory is shown in Figure 2-16. Approximately 1 hour of data was collected, the portion of data chosen for analysis is highlighted, which is in head seas, and is approximately eight minutes. The closest wave buoy was approximately 20 km away from the test site. This was not close enough to describe the sea conditions at the test site accurately; also, the changes in water depth between the locations of the buoy and the test site would skew the results.

Experimental data for pontoon and suspension accelerations were recorded, accelerations at post locations are shown in Figure 2-17 with their running mean value. Fast Fourier transform (FFT) was performed on each of the post acceleration data sets, with results shown in Figure 2-18, yielding a dominant frequency of 0.73 Hz. The expected value (EV) and standard deviation were also calculated for each of the post acceleration data sets. The results from the FFT analysis and statistical analysis are summarized in Table 2-3. The average asymmetry of the experiment is also shown in Table 2-3 with a total average difference between the port and starboard sides being 9.6%.



Figure 2-16 Sea-trial trajectory for WAM-V rough -water testing and the direction of dominant waves

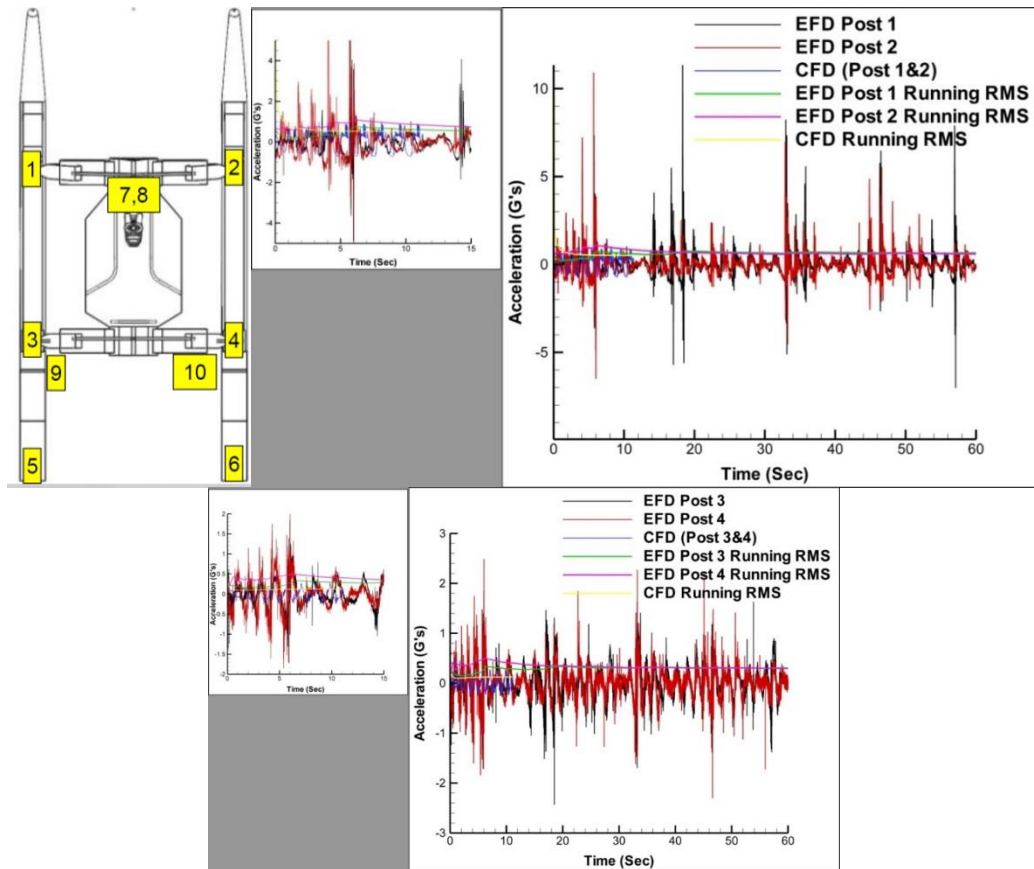
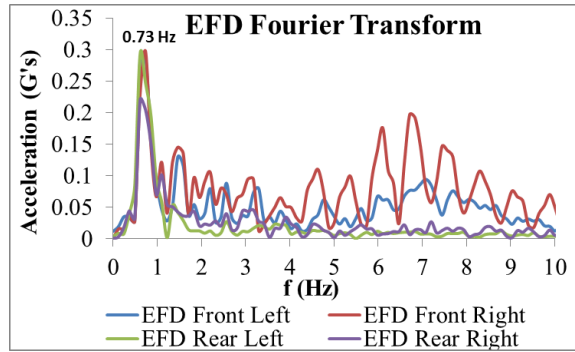


Figure 2-17 Comparison of time histories and running RMS for EFD and CFD accelerations at the front and rear posts



**Figure 2-18 FFT results for EFD accelerations at the front and rear posts**

**Table 2-3 Statistical results for rough-water testing**

Acceleration		EFD (Irregular Waves)		
		Left	Right	Diff (%)
Pontoon Front	EV(G's)	-0.012	-0.0011	-
	SD (G's)	0.47	0.63	29.09
	Dom Freq (Hz)	0.733	0.733	0.00
	Dom Amp (G's)	0.287	0.297	3.42
	Avg			10.84
Pontoon Rear	EV (G's)	0.004	-0.0011	-
	SD (G's)	0.35	0.32	8.96
	Dom Freq (Hz)	0.733	0.733	0.00
	Dom Amp (G's)	0.24	0.20	18.18
	Avg			8.43
Pontoon Average	Avg			9.64

## CHAPTER 3 COMPUTATIONAL METHODS

### 3.1 Overview of CFDShip-Iowa Version 4.5

CFDShip-Iowa V4.5 is a high-fidelity incompressible URANS/DES solver designed for ship hydrodynamics [8]. Single-phase level-set approach is used for free surface, blended  $k\text{-}\varepsilon/k\text{-}\omega$  for turbulence model, and curvilinear dynamic overset grids for 6DoF ship motions. An MPI-based domain decomposition approach is used, where each decomposed block is mapped to one processor. All equations of motion are solved in a sequential form and iterated to achieve convergence within each time step.

For the friction studies for 1DoF cylinder drop, a linear damping is added to the motions solver proportional to the vertical velocity:

$$m\ddot{z} = Z - C_F\dot{z} \quad (1)$$

where  $m$  is the total mass,  $\dot{z}$  the heave velocity,  $\ddot{z}$  the heave acceleration,  $Z$  the heave force, and  $C_F$  the friction coefficient.

#### 3.1.1 Two-Body Dynamics for Hinged Engine Pod

A two body dynamic model is implemented into CFDShip-Iowa to predict the rigid body motions of the pontoon and the hinged engine pod [6]. For hinged engine pod simulations, the rotation of the pod adds an additional degree of freedom. A block diagram (Figure 3-1) shows the method in which the two-body dynamics model is coupled into the existing CFDShip-Iowa method. The forces and moments are computed by integration of the forces on the solid surface including the forces caused by gravity. The engine pod is constrained by the hinge at the end of the pontoon and follows the pontoon motions except

that it is free to rotate about the y-axis. Two pitching moments are computed, one about the center of rotation of the WAM-V, and one about the hinged axis of rotation of the engine pod. The rotation of the engine pod is solved using

$$k \frac{d^2\phi}{dt^2} = M_{pod} \quad (2)$$

where  $k$  is the moment of inertia of the engine pod.

The integrations of the 6DoF equations of motion are executed using an implicit predictor-corrector method for the pontoon and an explicit method for engine pod. The predictor uses an explicit method, using forces and moments calculated from the current time-step to guess the solution at the next time step. The engine pod rotations for the next time-step are solved at the end of the current time-step, and are calculated only once per time-step. For pontoon, the corrector step is added at the end of each non-linear iteration using the predicted engine pod rotation.

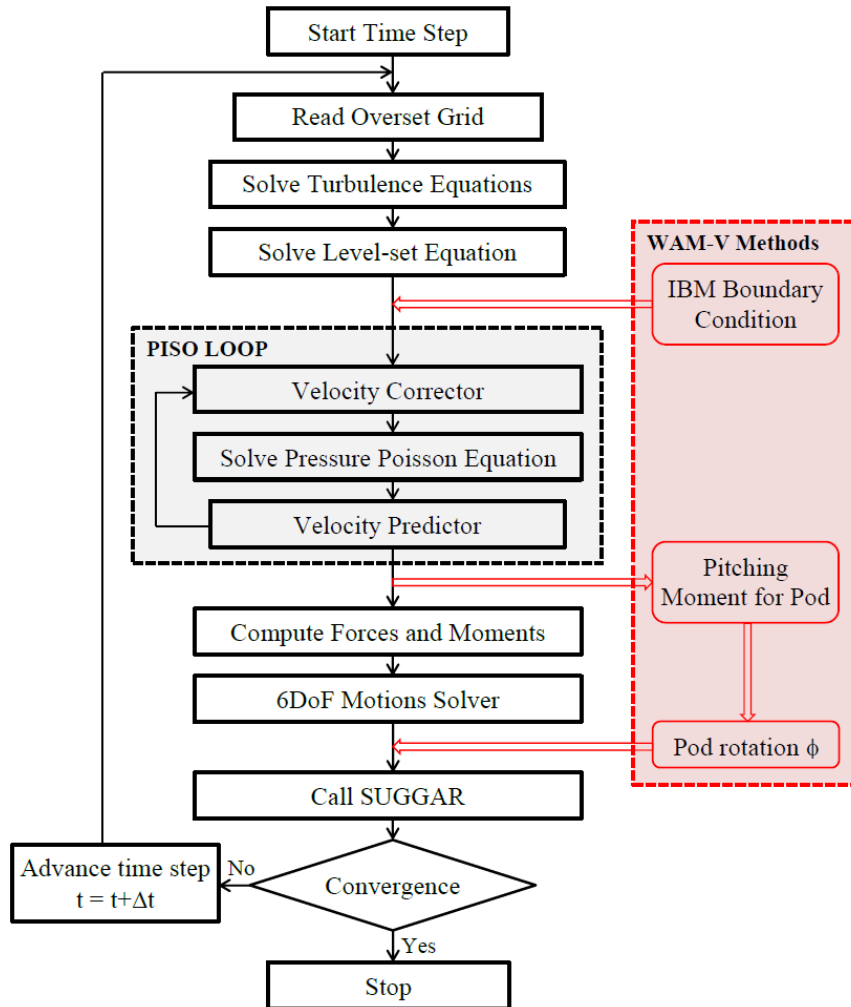


**Figure 3-1 Block diagram for two-body dynamics model for hinged engine pod simulations [6]**

### 3.1.2 LS-IBM for Pontoon-Pod Gap

A level-set immersed boundary method is implemented into CFDShip-Iowa to prevent flow into the gap between the pontoon and the engine pod [6]. Simulation of flows between small gaps is prone to numerical instability and the issues are compounded if the free surface is involved. A cylindrical surface grid is implemented into the gap region, starting at the trailing edge of the pontoon, extending to the leading edge of the engine pod. For this surface the level-set is specified to be zero if less than zero, i.e. the free surface



follows the cylindrical grid in the submerged region. The LS-IBM implementation onto the WAM-V pontoon-pod gap is shown in Figure 3-2.

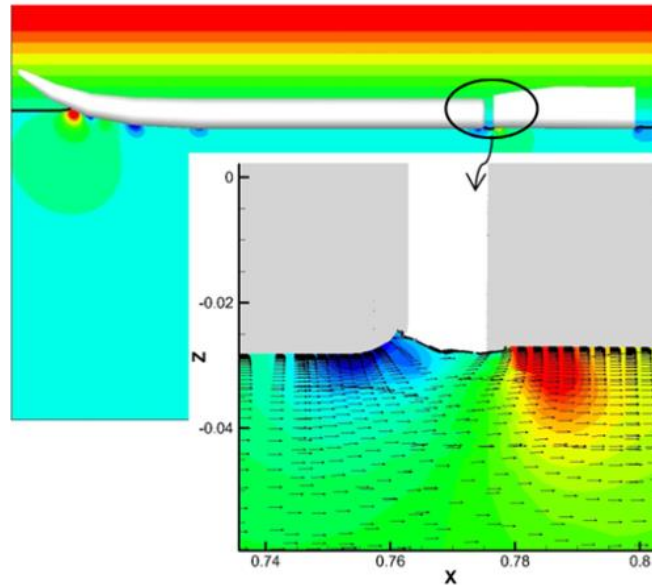


**Figure 3-2 Level-set immersed boundary method (LS-IBM) implemented to treat the flow inside the gap**

### 3.1.3 Jet Force Model for Validation against Free-Running Experiments

A waterjet model is implemented for free-running validation capabilities. For calm water simulations at each Froude number, the instantaneous jet-force is set equal to the instantaneous total resistance. Three to five non-linear inner iterations are carried out at each time-step to converge on jet-force, flow field, pontoon motions, and engine pod motions before marching to the next time-step. Calm water simulations are run until steady-state solutions are obtained for all forces and motions. For simulations in waves, a constant jet-force value is used based on the steady state calm water result at the same speed. Although the magnitude of the jet-force is constant during simulations in waves, the action

line changes according to the instantaneous pontoon and hinged engine pod motions, inducing time varying forces and moments.

### **3.2 Simulink Multi-Body Dynamics**

MBD models are created for cylinder drop and WAM-V using Matlab Simulink [16]. For cylinder drop, an actuator post inputs the vertical motion of the pontoon to the virtual model of the suspension system that predicts the induced sprung mass motions and the vertical force exerted on the un-sprung mass. For WAM-V, a six-post MBD model is created, named after the six actuator posts under the WAM-V in the model; four actuators support the pontoons (front and rear, right and left) and two support the engine pods. A diagram of the 6-post model is shown in Figure 3-3 with the model inputs and the total degrees of freedom. Models are created for each individual suspension setup, i.e. one model for the first generation suspension and one model for the second generation suspension.

The vertical forces at each actuator post are provided by the MBD model and are used for coupling with CFD. For suspension motions, the model is capable of outputting data from all the sensor locations from the sea-trials testing. The 6-post model is also equipped with a visualization package that runs through Simulink to provide qualitative comparisons of the simulation outputs. Table 3-1 summarizes the input variables into the WAM-V MBD code.

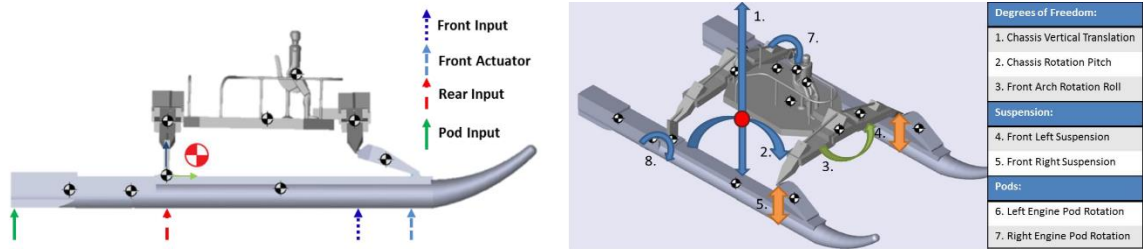


Figure 3-3 WAM-V MBD model: Input motions (left) and total degrees of freedom (right)

Table 3-1 - Input variables for MBD code

Front Post Motions	LF_Displ	Left front displacement
	RF_Displ	Right front displacement
	LF_Vel	Left front velocity
	RF_Vel	Right front velocity
	LF_Acc	Left front acceleration
	RF_Acc	Right front acceleration
Rear Post Motions	LR_Displ	Left rear displacement
	RR_Displ	right rear displacement
	LR_Vel	Left rear velocity
	RR_Vel	right rear velocity
	LR_Acc	Left rear acceleration
	RR_Acc	right rear acceleration
Engine Pod Motions	RP_Displ	Right engine pod displacement
	LP_Displ	Left engine pod displacement
	RP_Vel	Right engine pod velocity
	LP_Vel	Left engine pod velocity
	RP_Acc	Right engine pod acceleration
	LP_Acc	Left engine pod acceleration

### 3.3 CFD-MBD Coupling

CFDShip-Iowa and the Matlab Simulink MBD code are coupled both for cylinder drop and WAM-V. The procedures below are similar for cylinder drop and WAM-V, only that cylinder drop includes only one actuator post, while the WAM-V coupling includes six posts. The block diagrams for one-way and two-way coupling are showed in Figure 3-4.

One-way coupling includes the effects of post motions on the upper structure, but the CFD code is not affected by the MBD response. As described above, CFDSHIP-Iowa has an internal implicit 6DoF motion solver which performs non-linear inner iterations at each time-step. The total weight as well as the weight of the hinged engine pod (for WAM-V only) needs to be specified as input to this motion solver. The MBD model is modified to be able to read the output motion file from CFDSHIP-Iowa, convert the center of gravity motions to post motions, and use the time history of post motions, from the beginning of the simulation, to calculate the time history of suspension response. In one-way coupling, the MBD model is called once the CFDSHIP-Iowa solution is complete.

Two-way coupling is implemented by iterating at each time-step to achieve convergence between the CFD and MBD responses. The CFDSHIP-Iowa motion solver is modified to incorporate additional force and moment components imposed by the MBD model. The Simulink code is compiled on high-performance computing (HPC) machines and is called from inside CFDSHIP-Iowa code several times at each time-step. Each time called, the MBD code uses the time history of the post motions, from the beginning of the simulation, to calculate the current suspension response and send the instantaneous vertical force and pitching moment (for WAM-V only) back to CFDSHIP-Iowa. The procedure is repeated until the solutions are converged, before marching to the next time-step.

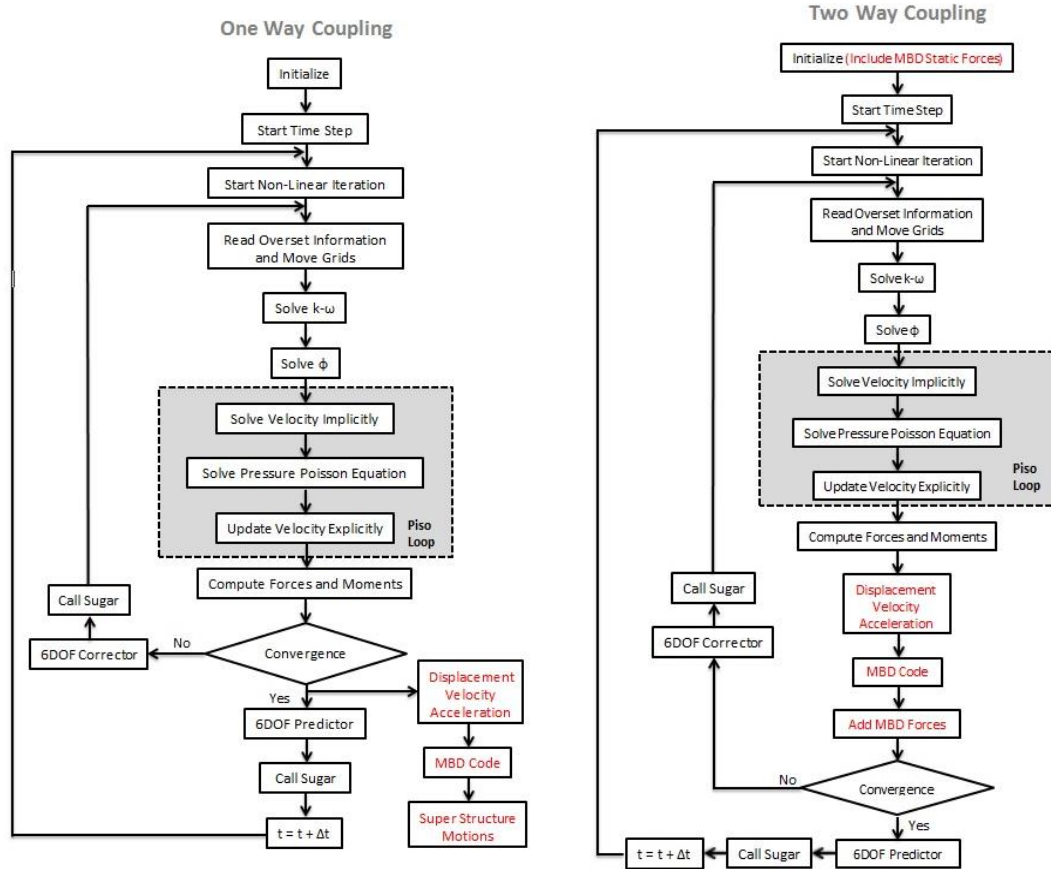
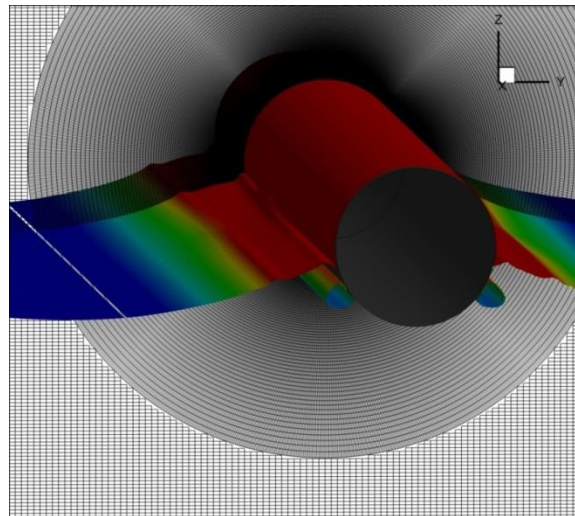


Figure 3-4 Block diagrams for CFD-MBD one-way (left) and two-way (right) coupling

## CHAPTER 4 SIMULATION CONDITIONS AND VALIDATION APPROACH

### 4.1 Cylinder Drop

Cylinder drop grid design is shown in Figure 4-1. A semi-2D grid is used with only 5 grid points in the third direction and periodic boundary conditions. The overset grid design allows for earth-fixed absolute inertial reference frame simulations in which the cylinder is dropped with initial zero velocity at time zero. The equations of motions are solved at each time step to move the cylinder body. The background grid is fixed while the body-fitted grid moves with the cylinder.



**Figure 4-1 Snapshot of grid and free-surface during a 1DoF cylinder drop simulation**

#### 4.1.1 Drop Height Determination

The drop heights to be used in simulations are determined based on analysis of the experimental data. A point-by-point average for the time histories of pontoon displacement is obtained at each drop height using the two repeated drop data. The average displacement data is then numerically differentiated to obtain pontoon velocity, using a numerical

smoothing to reduce high frequency oscillations. The drop height is determined based on the pontoon velocity at the impact with the free-surface, using frictionless free-fall kinematic equations. Table 4-1 shows the corrected drop heights for 1DoF and 2DoF cylinder drop tests.

**Table 4-1 Corrected drop heights for CFD grid correction**

Drop Number	Original Drop Height [m]	$t_{\text{impact}}$ [s]	Corrected Drop Height [m]	Percent Difference
09	0.30	0.19756	0.19145	36.2
10	0.30	0.19488	0.18628	37.9
11	0.37	0.22890	0.25700	30.5
12	0.37	0.22887	0.25693	30.6
21	0.30	0.20213	0.20041	33.2
22	0.30	0.19375	0.18412	38.6
23	0.37	0.23155	0.26299	28.9
24	0.37	0.22760	0.25409	31.3

#### 4.1.2 V&V Grid and Time-step

The CFD V&V studies for 1DoF cylinder drop include grid and time-step convergence studies. The grid study is conducted for coarse, medium, and fine grids with total grid points of 262k, 407k, and 697k, respectively. Time-step studies are carried out with time-step sizes of 0.001s (1 kHz), 0.0005s (2 kHz), and 0.00025s (4 kHz). All other simulations are carried out with fine grid (700k) and medium time-step (2 kHz).

#### 4.1.3 Friction Studies

The linear friction studies are carried out for CFD simulations of 1DoF cylinder drop with  $h=0.26$  m. Other than the friction-less simulation and a simulation with very small friction coefficient ( $C_F=0.05$ ), three systematic friction coefficients are included with a growth ratio of 2.0 ( $C_F=0.525$ , 1.05, and 2.10).

#### 4.1.4 Validation Approach

Validation parameters are the local extrema (peak#1, trough#1, etc.) values and their corresponding times for pontoon displacement ( $z_p$ ;  $t_p$ ) and suspension displacement ( $z_s$ ;  $t_s$ ). The first trough and first peak are used for 1DoF V&V studies for grid and the first four extrema are used for time-step. Grid studies are limited to the first two extrema due to computational expenses. Four extrema are used for 1DoF drop (two troughs and two peaks) and five extrema for 2DoF (three troughs and two peaks).

V&V studies are performed for grid and time-step studies to determine the uncertainty in the grid sizing ( $U_g$ ) as well as the time-step sizing ( $U_t$ ) for CFD simulations. To evaluate these uncertainties as percentages ( $U_g\%S_{1R}$ ;  $U_t\%S_{1R}$ ), the uncertainty values are divided by the smallest grid and smallest time step resolution simulation ranges ( $S_{1R}$ ), with the range being from the time of impact with the free-surface to the last extrema consider.

EFD uncertainty values ( $U_D$ ) are obtained for the extrema amplitudes and corresponding times. Equal upper and lower bounds are defined, about the average, as the difference between the two repeated drops. Data range (DR) values are used for calculating percent error values, the range being from impact with free-surface to the last extrema considered.

Validation for un-coupled CFD is carried out using 1DoF EFD experiments, where validation parameters include pontoon only. For un-coupled MBD validation, the average 2DoF EFD pontoon motions are prescribed as actuator post input to MBD. This is called EFD-MBD, where validation parameters include suspension only. For CFD-MBD,



validation parameters include both pontoon and suspension, where each of the error values include coupled contributions from CFD modeling and numerical errors, MBD modeling and numerical errors, and numerical errors from CFD-MBD coupling.

## **4.2 Shaker Rig MBD Validation**

MBD validation studies were carried out for WAM-V using scaled CFD results as base excitation into shaker rig experiment. CFD simulation results for rough water, with a wave length of  $\lambda/L=1.33$  and a wave height of  $H/\lambda=1/64$ , are scaled and the coordinates translated to the shaker rig posts. The shaker rig is then excited by the scaled CFD motions and the accelerations and displacements of the pontoons and suspension are recorded. The suspension displacement is used as the validation variable for WAM-V MBD.

## **4.3 WAM-V Sea-Trials**

A half domain grid of 2.3M grid points is used, exploiting the symmetry condition. The hull geometry, domain, and the overset grid system are shown in Figure 4-2. The Cartesian background grid extends enough to the sides and behind the ship ( $-0.5 < x/L < 3.5$ ;  $-1.3 < y/L < 1.3$ ) to capture the free surface and wake flows. The water depth is  $z/L = -0.8$ , and the top boundary extends to  $z/L = 0.3$ . The boundary layer grid is designed to achieve  $y^+ < 1$ . Free surface grids are designed to include sufficient points per surface elevations and wavelengths in the range of the current simulations.

The simulation conditions are set up in collaborations with Virginia Tech to match the sea-trial test conditions, including the weights, centers of gravity, and radii of gyration of the major components; as well as the hinge axis for hinged engine pods, the jet nozzle

locations and angles, and the hydrostatic sinkage, trim, and engine pod rotations. The engine pods are able to move through -2 to +15 degrees of travel in CFD-MBD simulations. Simulations are carried out in a relative inertial coordinate system fixed to the ship moving at constant-speed.

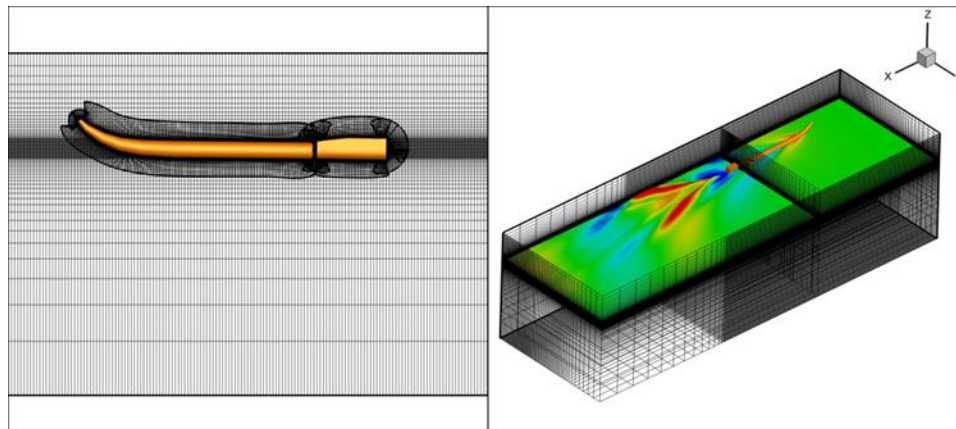


**Figure 4-2 Overset grid (left) and half-domain design (right) for WAM-V simulations**

### 4.3.1 Calm Water Simulation

#### *4.3.1.1 Hydrostatic Setup*

Ship model properties including masses and locations of centers of gravity for all components are provided by VTec, and CFD setup conditions are determined collaboratively in order for CFD hydrostatic simulation results to match experimental hydrostatic conditions. For 2-way coupled simulations, the hydrostatic setup procedure includes determining the pre-loads in the suspension system and including in the model as a force and moment offset, to achieve the EFD hydrostatic conditions. The hydrostatic force and moment offsets are applied for all 2-way CFD-MBD WAM-V simulations at speeds.

#### *4.3.1.2 Validation Approach*

For calm water, only one validation parameter is available, i.e. relative pontoon angle. EFD values are averaged between the right and left engine pod angles. Uncertainty values are obtained with equal upper and lower bounds, as the difference between the two values. The DR value is defined as the difference between the minimum and maximum engine pod angle for the Froude range.

### 4.3.2 Single-Wave Simulation

#### *4.3.2.1 Input Waves for Validation Simulation*

As for rough-water testing, the incoming waves were not measured during the single-wave encounter. A visual estimate of the waves is provided as 48 inch tall wave, with an estimated wavelength approximately equal to the length of the WAM-V [16]. Analysis of the pontoon motion data (Figure 4-4, left) as well as experimental video showed that the ship goes through a wave before and a wave after the large wave. The incoming wave design was started from a regular wave, consisting of three peaks and two troughs, as shown in Figure 4-3 (middle) in dashed line. The amplitudes and the wavelengths for each piece were then scaled according to their counterpart ratios in the pontoon displacement data, as shown in solid line in Figure 4-3 (middle). To generate the waves inside the computational domain, a non-dispersive wave-packet is designed, as shown in Figure 4-3 (right). The wave-packet is generated by superimposing a finite number of regular wave components based on the Fourier reconstruction of the desired input repeating with a distance of four ship lengths in between. CFDSHIP-IOWA uses the wave component information to calculate and prescribe the wave field as initial and

boundary conditions. For detailed description of input wave procedures refer to Mousaviraad et al. [11].

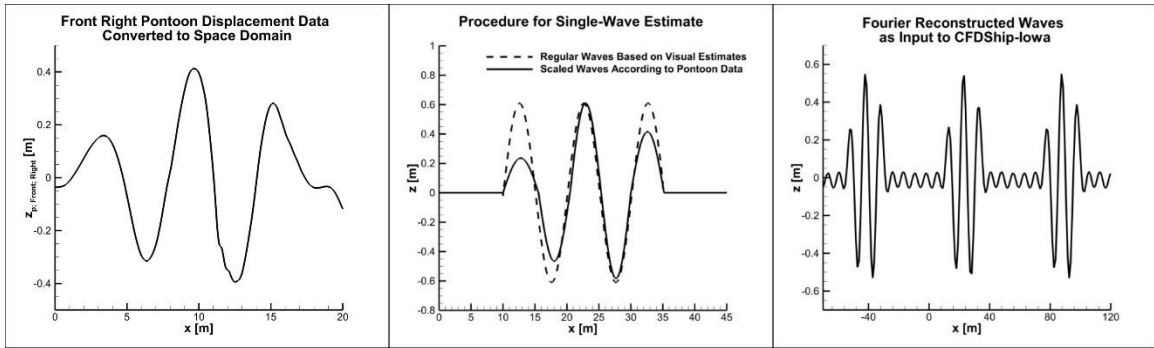


**Figure 4-3 Procedure to design an estimate wave group as input to CFDShip-Iowa for the single-wave validation simulation**

#### 4.3.2.2 Validation Approach

For single-wave, validation parameters are the local extrema values and their corresponding times ( $z_{pF}$ ;  $t_{pF}$ ;  $z_{pR}$ ;  $t_{pR}$ ;  $z_s$ ;  $t_s$ ). Three extrema are used, i.e. the large peak and the troughs before and after. For DR values, the range is from the initial small peak to the last extrema considered. Validation of CFD without coupling could not be performed since no WAM-V sea-trial data were available with suspension locked out. Similar to 2DoF cylinder drop, EFD-MBD results are obtained to evaluate the accuracy of MBD.

### 4.3.3 Rough Water Simulation

#### 4.3.3.1 Input Waves for Validation Simulation

The environmental waves were not measured during the WAM-V sea-trials. The conditions were visually estimated as head seas with some bow-quartering waves in sea-state 2 to 3 [16]. To determine the simulation conditions in CFDShip-Iowa, the data from the sea-trial testing program was analyzed. Evaluating the depth trace, a depth of 26.4 feet

was used. Statistical analysis of the pontoon accelerations was conducted to provide an estimate of the dominant encounter frequency. Regular head waves at the dominant encounter frequency ( $f_e=0.73$  Hz;  $\lambda/L=1.33$ ) and with a wave height over wavelength of  $H/\lambda=1/64$ , the typical value for sea-state 3, was used as input waves. Note that the sea waves were irregular and not unidirectional. The regular waves in simulations are designed to be representation of the seas, and not an exact reproduction.

#### *4.3.3.2 Validation Approach*

For rough-water, validation parameters are the SD, dominant frequencies, and dominant amplitudes of front and rear pontoon and suspension accelerations. EV are near zero and not included as validation parameters. EFD pontoon accelerations are asymmetric, while CFD results are symmetric. Error values are evaluated using both right and left data individually, and then averaged. Data values (D) are used for percent error calculations.

## CHAPTER 5 CFD V&V FOR 1-DOF CYLINDER DROP

### 5.1 Grid and Time-step Verification Results

The results for grid and time-step verification studies are shown in Table 5-1, where the uncertainties for the first four extrema are averaged together and reported. For grid studies, the average grid uncertainty for pontoon amplitude is  $U_g=2.35\%$ , the average grid uncertainty for pontoon time is  $U_g=2.06\%$ , with a total average grid uncertainty of  $2.20\%S_1R$ . For time-step studies, the average time-step uncertainty for pontoon amplitude is  $U_t=2.97\%$ , the average time-step uncertainty for time is  $U_t=0.43\%$ , with a total average time-step uncertainty of  $1.70\%S_1R$ .

**Table 5-1 CFD verification and validation (V&V) results for 1DoF cylinder drop**

		Grid Convergence				Time-Step Convergence				Validation			
		r	R	P	$U_g$ (%S <sub>1</sub> R)	r	R	P	$U_t$ (%S <sub>1</sub> R)	$U_{SN}$ (%S <sub>1</sub> R)	$U_D$ (%DR)	$U_V$ (%DR)	E (%DR)
Trough #1	$z_p$	2 <sup>1/2</sup>	-0.40	-	2.58	2	-0.02	-	4.72	5.06	1.26	5.21	2.95
	$t_p$		0.18	4.93	0.95		-0.03	-	1.20	1.58	0.43	1.66	1.56
	Avg				1.77				2.96	3.32	0.85	<b>3.44</b>	<b>2.25</b>
Peak #1	$z_p$		-0.31	-	3.42		-0.27	-	3.98	4.98	9.05	10.33	28.92
	$t_p$		8.68	-6.23	-		1.8E-04	6.22	1.8E-05	1.9E-05	2.27	2.27	4.26
	Avg				3.42				1.99	2.49	5.66	<b>6.30</b>	<b>16.59</b>
Trough #2	$z_p$		-0.34	-	2.05		-0.51	-	2.41	3.00	0.35	3.02	8.92
	$t_p$		-0.07	-	1.75		0.05	2.15	0.42	1.79	1.58	2.41	3.44
	Avg				1.90				1.42	2.40	0.97	<b>2.72</b>	<b>6.18</b>
Peak #2	$z_p$		-0.38	-	1.34		-0.77	-	0.75	1.48	7.11	7.26	16.14
	$t_p$		0.20	4.63	3.48		0.02	2.92	0.09	3.45	4.55	5.74	7.94
	Avg				2.41				0.42	2.46	5.83	<b>6.50</b>	<b>12.04</b>
Avg	$z_p$			2.35			2.97	3.63	4.44	6.46	14.23		
	$t_p$			2.06			0.43	1.70	2.21	3.02	4.30		
	Avg			<b>2.20</b>			<b>1.70</b>	<b>2.67</b>	<b>3.32</b>	<b>4.74</b>	<b>9.27</b>		

## 5.2 Friction

The results for linear friction studies to compensate for friction in the guide rails are shown in Table 5-2 and Figure 5-1. The effects of friction are significant, reducing the total average error from  $E=7.35\%$  to  $3.84\%$  DR for  $C_F=1.05$ . However, the results are not consistent, i.e. the error values increase for some of the extrema while they decrease for the other. This shows that a simple linear damping is not sufficient and more advanced modeling will need to be considered in the future, such as a bi-linear damping similar to what was used in SB modeling [16]. In the rest of the current cylinder drop simulations, no friction damping is included.

**Table 5-2 Linear friction coefficient studies for  
1DoF cylinder drop  $h=0.26[m]$**

Locked Out - 1DoF		E%DR				Avg
		Trough #1	Peak #1	Trough #2	Peak #2	
$C_F=0.00$	$z_p$	2.65	22.89	16.01	8.44	12.50
	$t_p$	0.87	2.29	2.55	3.07	2.19
	Avg	1.76	12.59	9.28	5.76	<b>7.35</b>
$C_F=0.05$	$z_p$	1.92	20.50	15.33	8.35	11.52
	$t_p$	0.73	1.96	2.02	2.44	1.79
	Avg	1.32	11.23	8.67	5.39	<b>6.65</b>
$C_F=0.525$	$z_p$	2.09	15.66	11.38	5.74	8.72
	$t_p$	0.82	0.64	0.49	0.04	0.50
	Avg	1.46	8.15	5.93	2.89	<b>4.61</b>
$C_F=1.05$	$z_p$	6.20	10.20	7.30	3.20	6.72
	$t_p$	1.01	0.54	0.99	1.27	0.95
	Avg	3.60	5.37	4.14	2.23	<b>3.84</b>
$C_F=2.10$	$z_p$	14.91	0.29	2.46	0.29	4.49
	$t_p$	1.16	2.69	4.63	6.13	3.65
	Avg	8.03	1.49	3.55	3.21	<b>4.07</b>

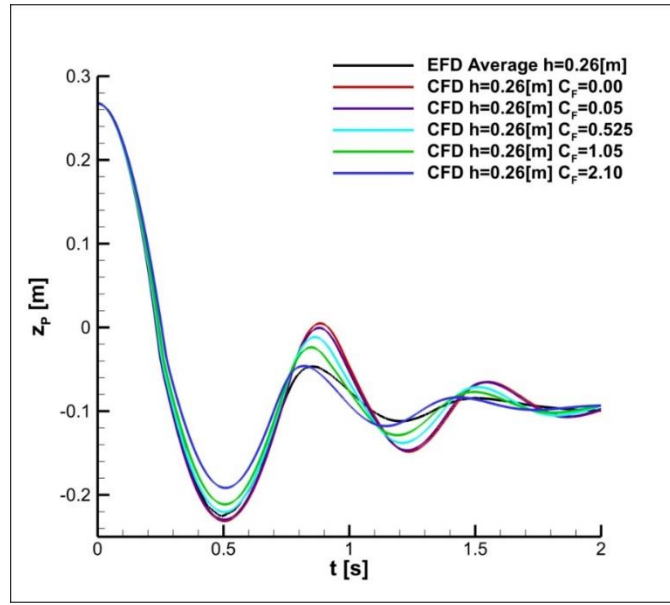


**Figure 5-1 Linear friction studies for 1DOF cylinder drop h=0.26[m] (EFD data from [16])**

### 5.3 Validation Results

CFD validation results for 1DOF cylinder drop are shown in Table 5-3 including comparison with SB. The uncertainty in the experimental data is  $U_D=3.12\%DR$ . The total average error values for CFD are  $E=5.9$  and  $9.3\%DR$  for  $h=0.20$  and  $0.26$  m, respectively. For SB, the error is smaller for the larger drop height, with an overall average of  $E=2.8\%DR$ . CFD is validated with an overall average of  $E=7.6\%DR$  for 1DOF cylinder drop.

CFD 1DOF results are plotted with the experimental data in Figure 5-2 and 5-3. A main feature of the physics involved is a sharp change in the slope of the pontoon displacement beginning at the time of impact. CFD-MBD pontoon displacement motions closely follow the experimental trends. The first troughs are within the EFD bounds for both drop heights, while the emergence magnitudes are over-predicted. The trough after emergence is predicted within the EFD bounds for  $h=0.20$  m, while for the higher drop



there are slight differences both for amplitude ( $z_p$ ) and time ( $t_p$ ). The suspension motions, relative to pontoon, are zero in CFD, while there are slight motions in EFD, which could have contributed to the validation error.

**Table 5-3 1DoF cylinder drop validation results**

Locked Out - 1DoF		E%DR				Avg
		Trough #1	Peak #1	Trough #2	Peak #2	
SB h=0.20[m]	$z_p$	4.16	9.92	9.59	0.30	5.99
	$t_p$	1.58	0.40	2.77	4.35	2.28
	Avg	2.87	5.16	6.18	2.33	<b>4.13</b>
CFD h=0.20[m]	$z_p$	4.62	14.38	2.72	16.30	9.51
	$t_p$	0.92	1.35	0.90	5.72	2.22
	Avg	2.77	7.87	1.81	11.01	<b>5.86</b>
SB h=0.26[m]	$z_p$	3.83	3.01	0.68	0.27	1.95
	$t_p$	1.37	0.34	1.14	1.59	1.11
	Avg	2.60	1.68	0.91	0.93	<b>1.53</b>
CFD h=0.26[m]	$z_p$	2.95	28.92	8.92	16.14	14.23
	$t_p$	1.56	4.26	3.44	7.94	4.30
	Avg	2.25	16.59	6.18	12.04	<b>9.27</b>
Average $U_D$ (%DR)	$z_p$	2.40	6.82	4.06	4.34	<b>4.41</b>
	$t_p$	0.24	1.56	1.17	4.40	<b>1.84</b>
	Avg	1.32	4.19	2.62	4.37	<b>3.12</b>
Average SB	$z_p$	3.99	6.47	5.14	0.29	3.97
	$t_p$	1.47	0.37	1.95	2.97	1.69
	Avg	2.73	3.42	3.55	1.63	<b>2.83</b>
Average CFD	$z_p$	3.78	21.65	5.82	16.22	11.87
	$t_p$	1.24	2.81	2.17	6.83	3.26
	Avg	2.51	12.23	3.99	11.53	<b>7.57</b>

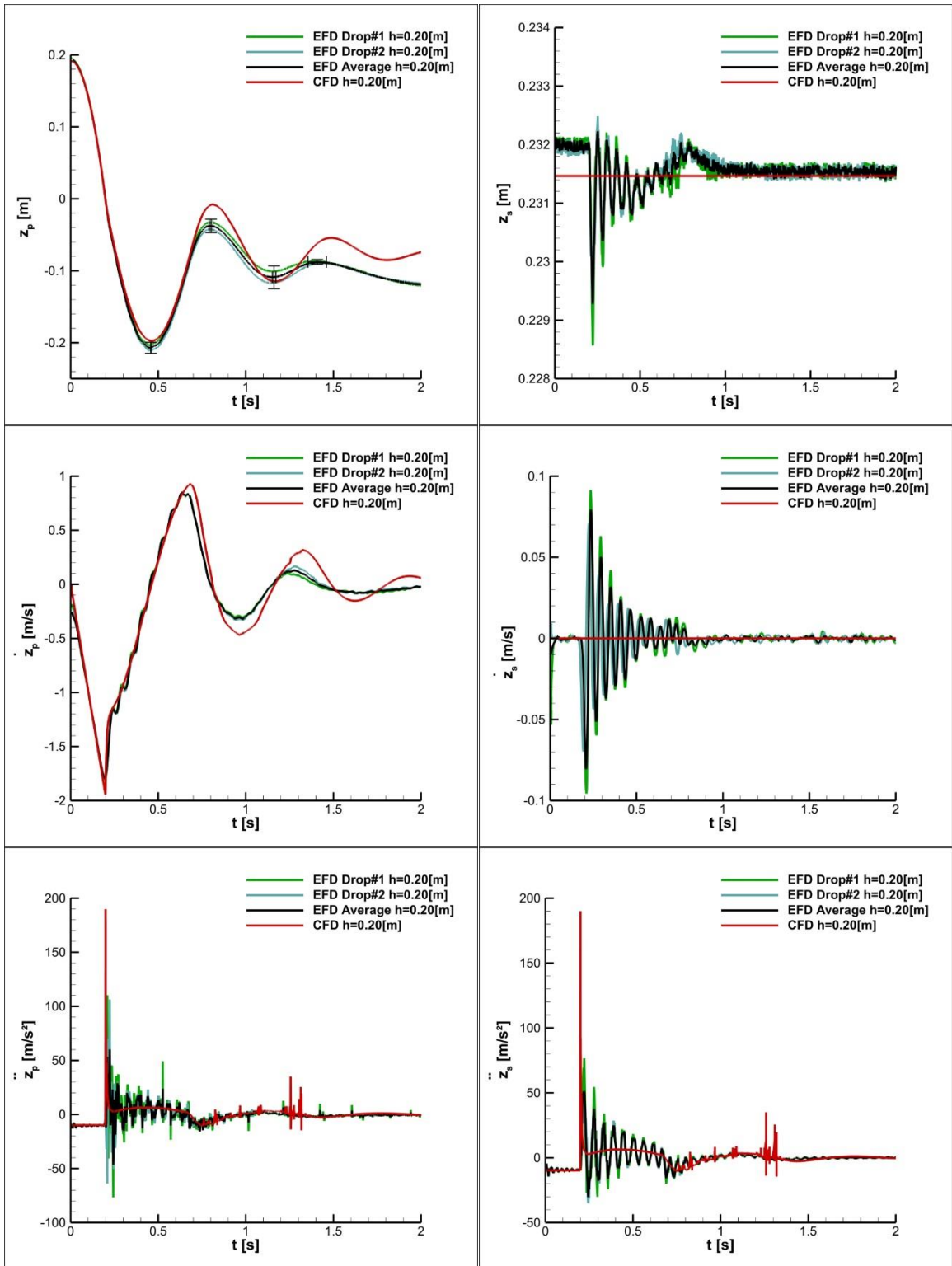


Figure 5-2 Validation results for 1DoF cylinder drop  $h=0.20\text{[m]}$  (EFD data from [16])

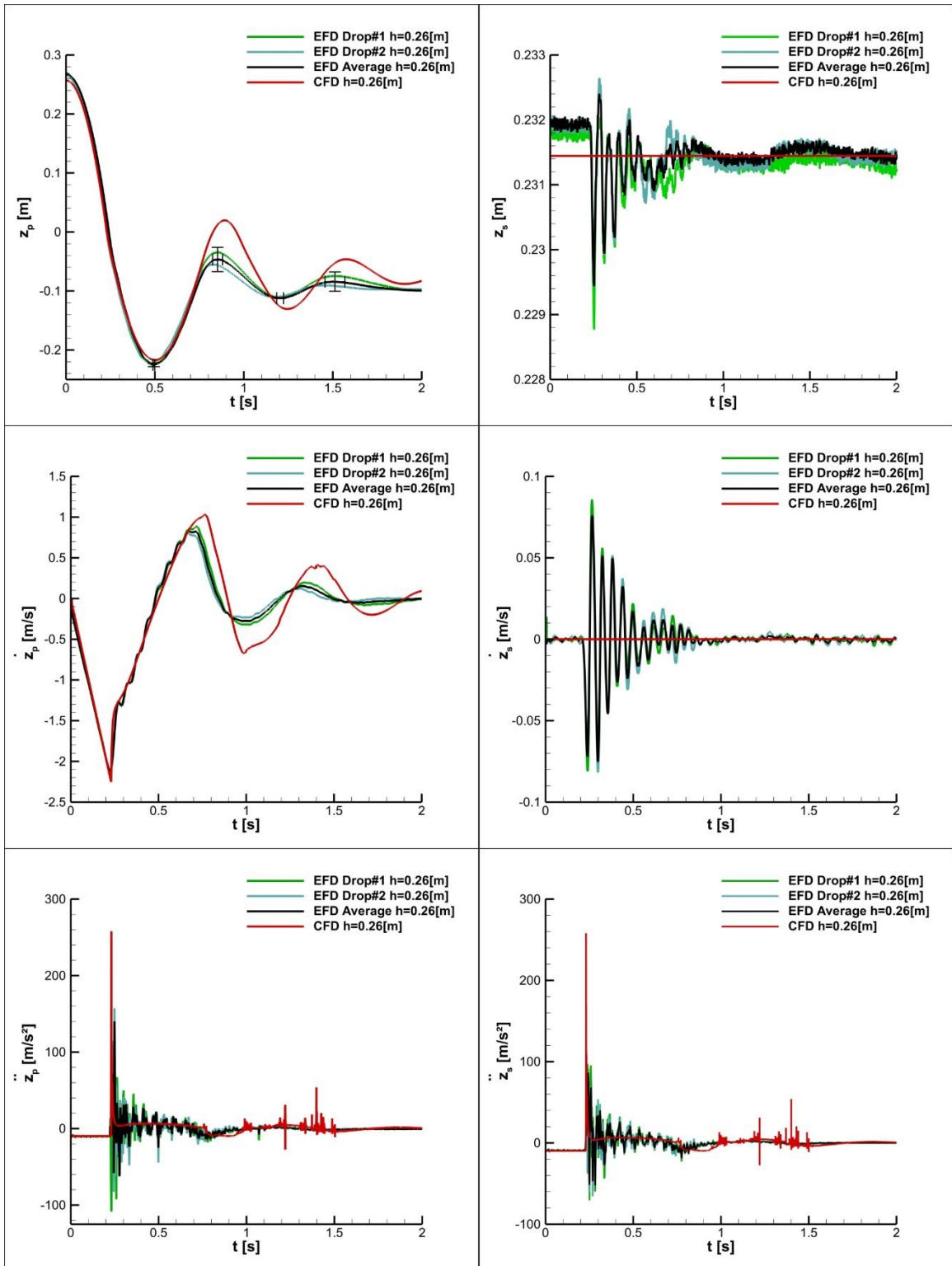


Figure 5-3 Validation results for 1DoF cylinder drop  $h=0.26$  [m] (EFD data from [16])

## CHAPTER 6 MBD VALIDATION RESULTS

### 6.1 WAM-V Un-Coupled MBD Validation against Shaker Rig Laboratory Experiment

Validation results for shaker rig study MBD validation study are shown in Figure 6-1. Predicted suspension displacement shows excellent agreement with EFD data. The troughs show a slight under prediction of amplitude, the peak amplitudes are predicted correctly, and the predicted frequency shows excellent agreement throughout the entire test.

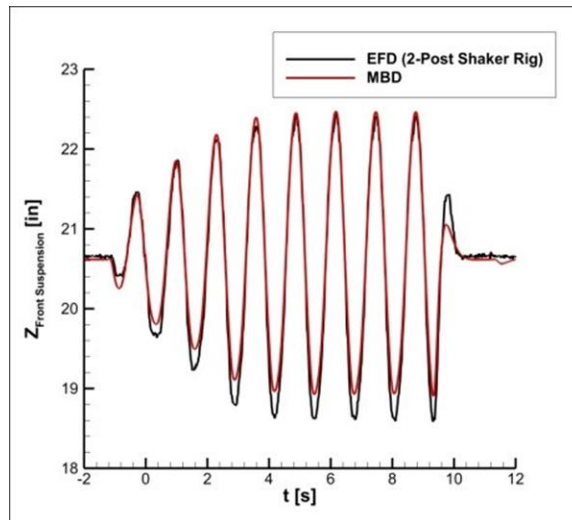


Figure 6-1 Validation of MBD code via 2-post shaker rig experiment (data from [16])

### 6.2 EFD-MBD for Un-Coupled MBD Validation against On-Water Data

#### 6.2.1 Cylinder Drop

Validation results for cylinder drop un-coupled MBD are shown in Figure 6-2 for  $h=0.20$  m (left) and for  $h=0.26$  m (right). The average suspension error over the two drop height simulations is 7.73%DR. This error is likely caused by friction in the guide rails

acting on the sprung mass. The suspension displacement is accurately predicted for the first trough for both drop heights. Both drop height simulations begin to lose accuracy at the first peak. The amplitude of the first peak and second trough are under predicted and the remaining predicted extrema follow the suspension displacement trends but fail to match amplitudes or frequencies. Friction in the guide rails should be modeled using a bi-linear or nonlinear friction model to improve MBD simulations [16].

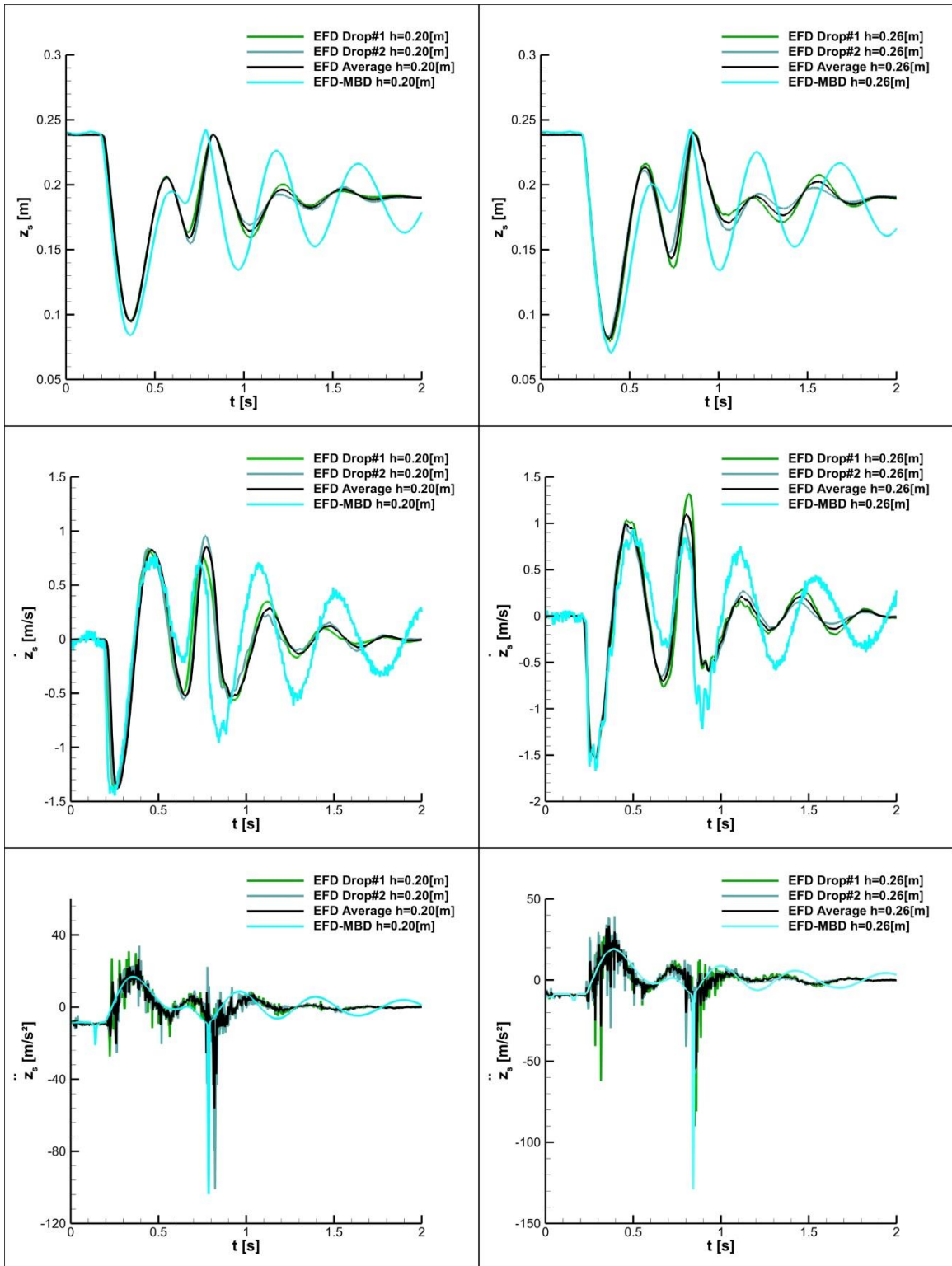
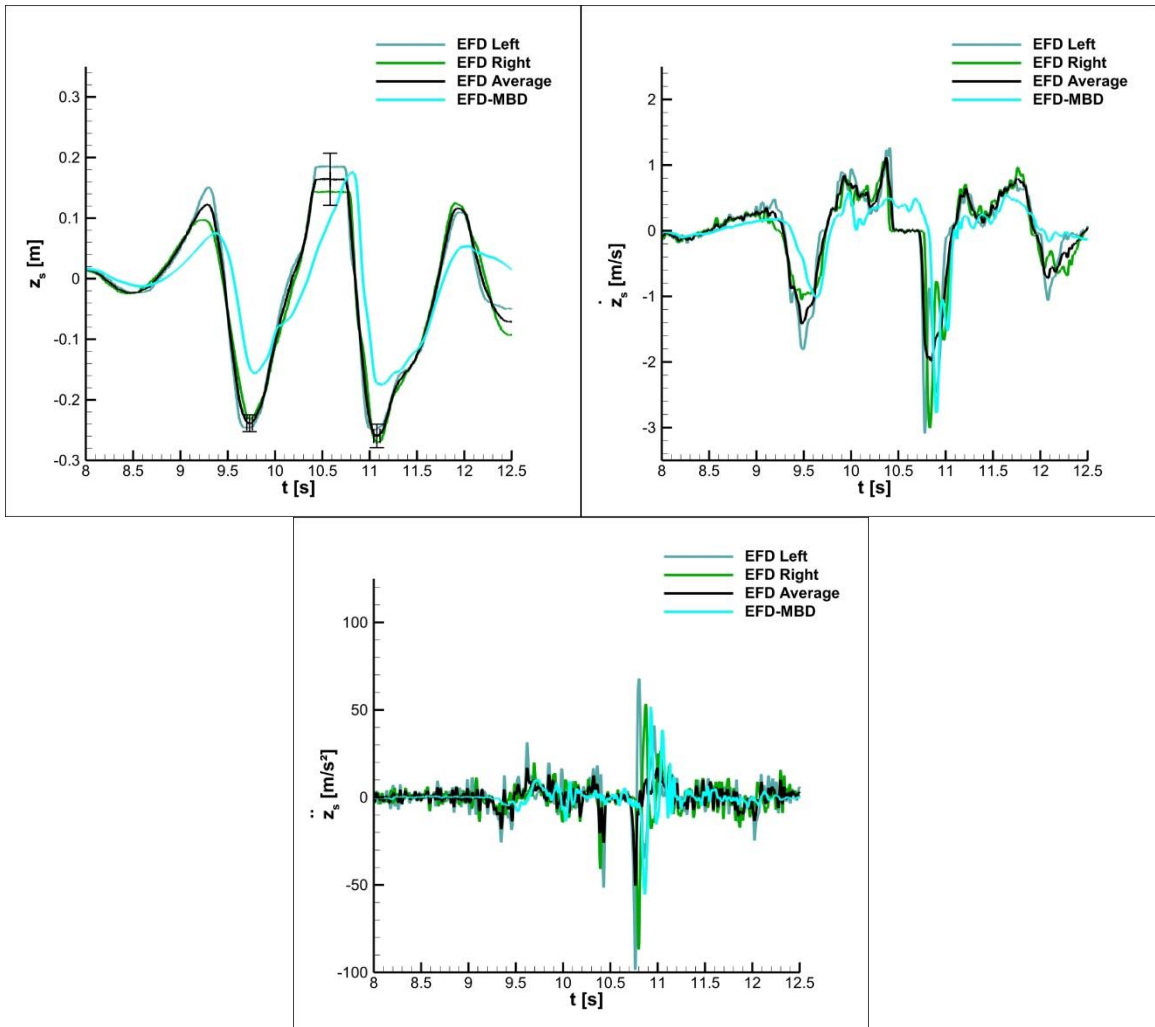


Figure 6-2 EFD-MBD validation results for 2DoF cylinder drop at  $h=0.20$  m and  $h=0.26$  m (EFD data from [16])

### 6.2.2 WAM-V Single-Wave

Validation results for WAM-V un-coupled MBD are shown in Figure 6-3. The average suspension error is 8.78%DR. The error in the suspension prediction is caused by imperfectly modeling the WAM-V suspension as a rigid base excitation problem. The flexing of the pontoons, as evident from experimental video footage of the single-wave test, is damping energy from the WAM-V motions. In the shaker rig experiment, the pontoons are strapped to the semi-rigid cradle, eliminating the flexing of the pontoon showing better suspension displacement predictions. The flexibility in the pontoon should be modeled using a finite element solver to accurately model the coupled physics.



**Figure 6-3 EFD-MBD validation results for single-wave simulation (EFD data from [16])**



## CHAPTER 7 CFD-MBD FSI VALIDATION RESULTS

### 7.1 2DoF Cylinder Drop

Validation results for 2DoF cylinder drop are shown in Table 7-1. The uncertainty in the experimental data for pontoon is  $U_D=4.02$ , suspension 2.41, with a total average uncertainty of 3.22%DR. For EFD-MBD, the overall average error is  $E=7.7\%$ DR (uncoupled MBD), comparable to CFD 1DoF validation error of  $E=7.6\%$ DR (uncoupled CFD), with SB 1DoF validation error being  $E=2.8\%$ DR (uncoupled SB). For SB-MBD, the overall average error is  $E=5.5\%$ DR, with component error values of  $E=3.8\%$ DR for pontoon and  $E=7.2\%$ DR for suspension. For CFD-MBD, the overall average error value decreases from  $E=16.3\%$ DR for 1-way coupling to  $5.6\%$ DR for 2-way, a 10.6% reduction. Component values are reduced by 7.2%DR for pontoon and 14.0% for suspension. For 2-way coupling, the results are validated with  $E=7.6\%$ DR for pontoon, same value as CFD 1DoF, and with  $E=3.7\%$ D for suspension. Overall, CFD-MBD 2-way coupling for 2DoF cylinder drop is validated with  $E=5.6\%$ DR.

The 2DoF CFD-MBD results are plotted with the experimental data in Figure 7-1 and 7-2. EFD pontoon displacements are significantly different from 1DoF: the angle of the slope change at the time of impact is larger, and a double peak is observed in the first emergence compared to a single peak in 1DoF. The CFD-MBD results show that a 2-way coupling is necessary to predict these physical features of a 2DoF drop, as they are both missed in 1-way simulations. For 2-way results, the first troughs are within the EFD bounds for both drop heights. The double peaks are over-predicted, consistent with 1DoF results where the emergence magnitudes were over-predicted. The troughs after emergence are predicted within the EFD bounds for both drop heights.

For suspension displacements, the CFD-MBD results show that the first troughs are over-predicted, both in magnitude and time, in 1-way simulations, whereas 2-way results show good agreement with EFD. The first peaks and the second troughs are completely missed by 1-way simulations, while 2-way results closely follow EFD. For the second peaks, 1-way simulations predict the amplitudes reasonably but the times are under-predicted. 2-way simulation results closely predict both the amplitudes and the times. The third troughs are over-predicted by 1-way and slightly under-predicted by 2-way, both for the amplitudes and the times.

**Table 7-1 2DoF Cylinder drop validation results**

Sprung - 2DoF		E%DR					Avg
		Trough #1	Peak #1	Trough #2	Peak #2	Trough #3	
CFD-MBD 1-Way h=0.20[m]	z <sub>p</sub>	10.42	32.48	35.72	32.22	4.53	23.08
	t <sub>p</sub>	23.64	4.28	4.31	13.88	6.51	10.53
	z <sub>s</sub>	15.56	25.13	57.54	2.06	14.13	22.88
	t <sub>s</sub>	6.79	17.90	9.74	13.10	9.45	11.40
	Avg	14.10	19.95	26.83	15.32	8.66	<b>16.97</b>
CFD-MBD 2-Way h=0.20[m]	z <sub>p</sub>	1.85	24.91	25.02	29.66	1.13	16.51
	t <sub>p</sub>	0.37	2.64	0.20	3.18	1.94	1.67
	z <sub>s</sub>	8.24	3.22	2.66	3.17	11.66	5.79
	t <sub>s</sub>	0.00	2.04	2.20	0.29	5.08	1.92
	Avg	2.61	8.20	7.52	9.07	4.95	<b>6.47</b>
CFD-MBD 1-Way h=0.26[m]	z <sub>p</sub>	8.51	29.56	32.17	25.14	7.46	20.57
	t <sub>p</sub>	3.50	7.12	0.32	10.42	3.66	5.00
	z <sub>s</sub>	13.76	15.52	54.03	4.38	32.74	24.09
	t <sub>s</sub>	7.28	15.27	11.88	9.14	18.99	12.51
	Avg	8.26	16.87	24.60	12.27	15.71	<b>15.54</b>
CFD-MBD 2-Way h=0.26[m]	z <sub>p</sub>	0.48	14.52	14.23	17.03	7.11	10.67
	t <sub>p</sub>	1.53	3.68	0.37	0.38	1.54	1.50
	z <sub>s</sub>	6.54	0.96	2.32	2.24	3.71	3.16
	t <sub>s</sub>	0.93	3.52	3.77	2.80	8.47	3.90
	Avg	2.37	5.67	5.17	5.61	5.21	<b>4.81</b>
Average U <sub>D</sub> (%DR)	Avg <sub>p</sub>	5.06	3.34	2.16	3.38	6.14	<b>4.02</b>
	Avg <sub>s</sub>	1.24	1.61	4.77	0.39	4.06	<b>2.41</b>
	Avg <sub>tot</sub>	3.15	2.48	3.47	1.88	5.10	<b>3.22</b>
Average EFD-MBD	Avg <sub>s</sub>	4.05	5.75	11.65	2.72	14.50	<b>7.73</b>
Average SB-MBD	Avg <sub>p</sub>	2.27	3.48	2.21	5.52	5.25	<b>3.75</b>
	Avg <sub>s</sub>	4.64	5.84	12.33	3.10	9.96	<b>7.17</b>
	Avg <sub>tot</sub>	3.45	4.66	7.27	4.31	7.61	<b>5.46</b>
Average CFD-MBD 1-Way	Avg <sub>p</sub>	11.52	18.36	18.13	20.42	5.54	<b>14.79</b>
	Avg <sub>s</sub>	10.85	18.46	33.30	7.17	18.83	<b>17.72</b>
	Avg <sub>tot</sub>	11.18	18.41	25.71	13.79	12.19	<b>16.26</b>
Average CFD-MBD 2-Way	Avg <sub>p</sub>	1.06	11.44	9.95	12.56	2.93	<b>7.59</b>
	Avg <sub>s</sub>	3.93	2.44	2.74	2.13	7.23	<b>3.69</b>
	Avg <sub>tot</sub>	2.49	6.94	6.35	7.34	5.08	<b>5.64</b>
Diff. (E <sub>1Way</sub> -E <sub>2Way</sub> )	Avg <sub>p</sub>	10.46	6.92	8.18	7.86	2.61	7.20
	Avg <sub>s</sub>	6.92	16.02	30.56	5.04	11.60	14.03
	Avg <sub>tot</sub>	8.69	11.47	19.36	6.45	7.11	10.62

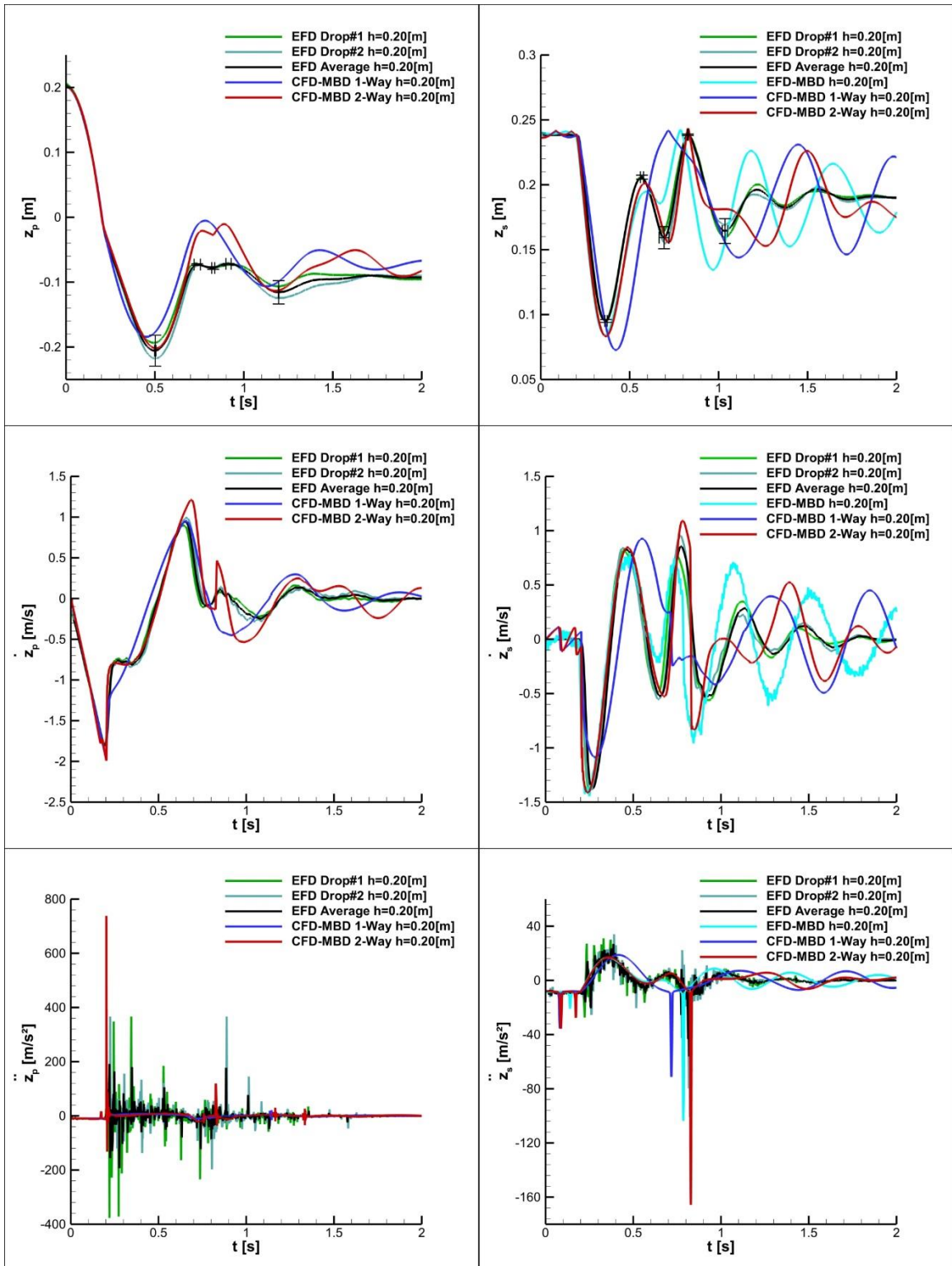


Figure 7-1 Validation results for 2DoF cylinder drop  $h=0.20\text{[m]}$

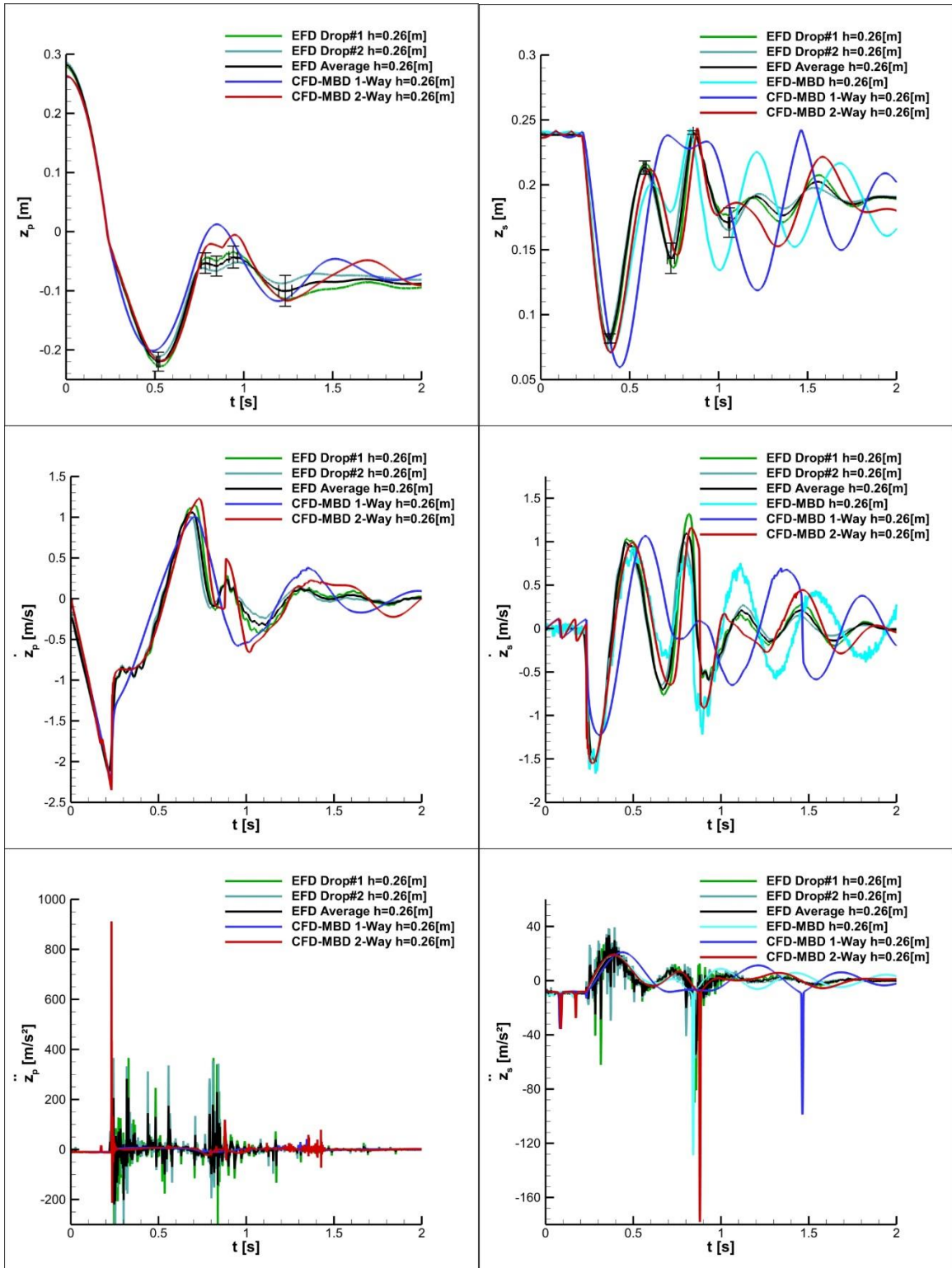


Figure 7-2 Validation results for 2DoF cylinder drop  $h=0.26\text{[m]}$

## 7.2 WAM-V Calm Water

Calm water validation results are shown in Table 7-2. Averaged over all Froude numbers, relative engine pod angle is validated with E=27.9% for 1-way and 14.2%DR for 2-way, with  $U_D$  being 6.8%DR. Compared to 1-way, error values are reduced by 13.7%DR on average, consistent with 10.6%DR reduction for 2DoF cylinder drop.

CFD-MBD 1-way and 2-way results are shown in Figure 7-3 and Figure 7-4. The effects of 2-way coupling compared to 1-way results are as follow. Sinkage shows a slight rise-up effect, except at  $Fr=0.0$ . Trim shows a bow-down effect, except at  $Fr=0.0$ , with a maximum at  $Fr=1.04$  being 0.8 degrees. Engine Pod angle has a downward pod rotation effect, except at  $Fr=0.0$ , with the maximum effect being 0.8 degrees at  $Fr=0.77$ . Total resistance coefficient does not change significantly. Suspension displacement has a downward relative motion effect, being maximum at  $Fr=1.04$  where 1-way predicts upward and 2-way predicts downward relative motion.

CFD-MBD 2-way simulations predict the vessel slightly sinks down at  $Fr=0.27$ , while it rises up at  $Fr=0.77$  and 1.04. Trim is bow-up at all  $Fr$ , being maximum at  $Fr=0.52$  with 1.4 degrees. Engine pod moves upward at speeds lower than  $Fr=0.52$  and downward at higher speeds. Maximum upward engine pod angle is about 1.5 degrees at  $Fr=0.27$ , and maximum downward pod angle is about 2.9 degrees at  $Fr=1.04$ . The relative front suspension displacement trend is similar to trim angle, being maximum upward for at  $Fr=0.52$ . At  $Fr=1.04$ , the suspension displacement is slightly negative.

**Table 7-2 WAM-V calm water validation results**

Fr	Engine Pod Angle (deg)				E%DR		
	Experiment		CFD-MBD		1-way	2-way	Diff. (E <sub>1Way</sub> -E <sub>2Way</sub> )
	D	U <sub>D</sub> (%DR)	1-way	2-way			
0.0	-1.15	8.59	-0.58	-1.13	12.77	0.45	12.32
0.27	0.27	2.58	-2.00	-1.46	50.48	38.88	11.60
0.77	3.26	3.00	1.98	2.79	28.58	10.56	18.02
1.04	3.30	12.86	2.42	3.00	19.68	6.74	12.94
Avg		<b>6.76</b>			<b>27.88</b>	<b>14.16</b>	13.72

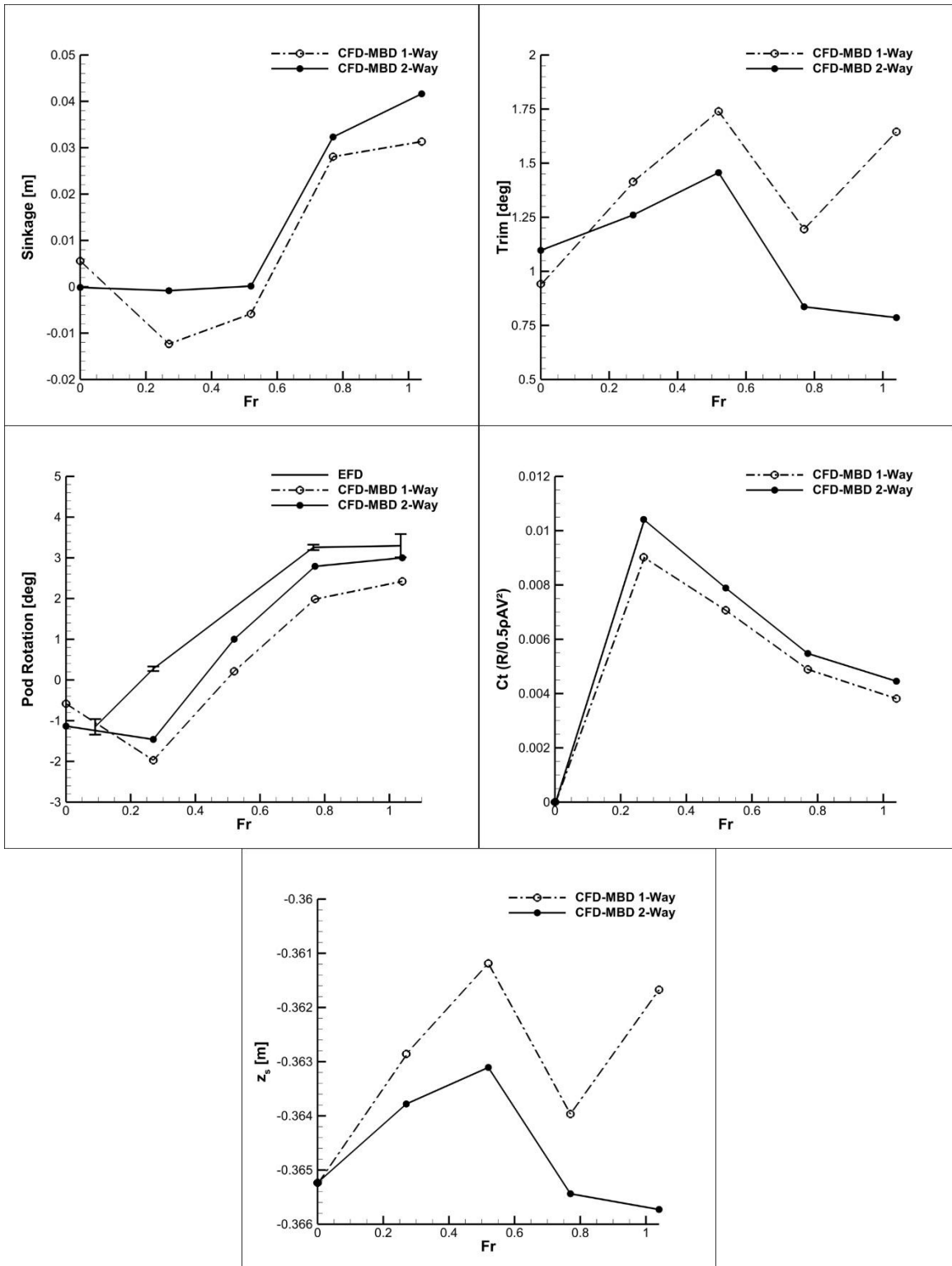


Figure 7-3 WAM-V calm water results



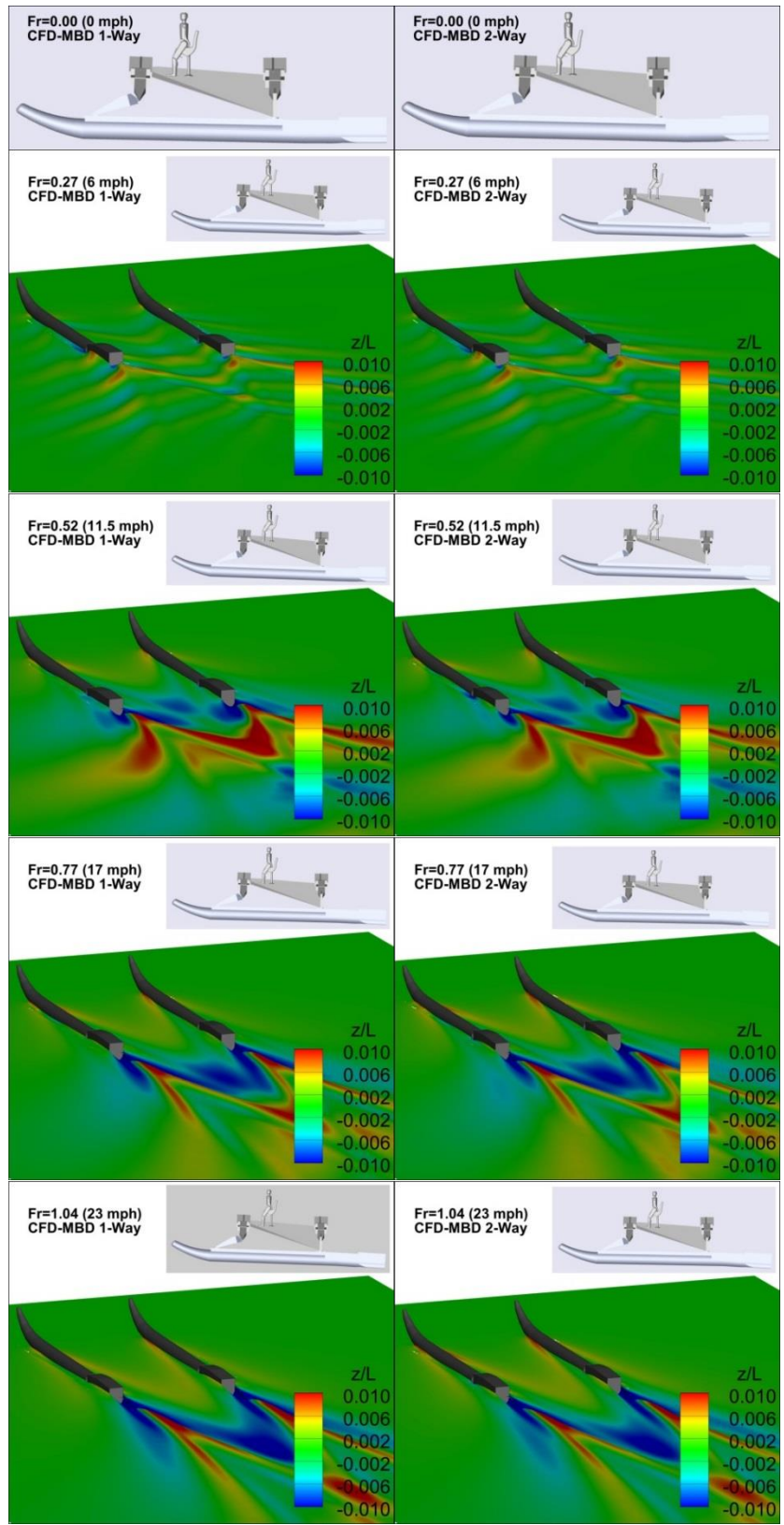


Figure 7-4 Free-surface and WAM-V motions for calm water simulations

### 7.3 WAM-V Single-Wave

Single-wave validation results are shown in Table 7-3. The total average uncertainty in experimental data is  $U_D=3.71$ , composed of 3.77 for pontoon and 3.59%DR for suspension. For EFD-MBD, the overall average error is  $E=8.8\%DR$  (un-coupled MBD), close to that of 2DOF cylinder drop being 7.7%DR. For CFD-MBD, the error values for average pontoon motions reduce from 16.3% for 1-way to 15.1%DR for 2-way. For suspension motions, the error values are 10.5% for 1-way and 20.8%DR for 2-way. The overall average error values for 1-way and 2-way are 14.4 and 17%DR, respectively. The differences between simulations and experiments are due to MBD errors, uncertainty in incoming waves, and the vessel speed reducing by 27% in experiment while held constant in simulations.

Pontoon and suspension motions are shown in Figure 7-5. For pontoon displacement, 2-way coupling significantly improves the simulation results for the large peak for the front post location. For pontoon displacement at the rear post location and suspension displacement, the trend is accurately predicted while the extrema amplitudes are under-predicted. Since the same under-prediction for suspension displacement is observed for the EFD-MBD results, the differences in CFD-MBD are speculated to be due to MBD error. The MBD model properties need to be updated to match the experimental conditions for future simulations. In Figure 7-6, snapshots of experimental videos and CFD-MBD free-surface and WAM-V motion predictions are shown for two different phases during the single-wave event.

**Table 7-3 WAM-V single-wave encounter validation results**

		E%DR			
		Trough#1	Peak#1	Trough#2	Avg
EFD U <sub>D</sub> (%DR)	Z <sub>pF</sub>	8.58	12.85	3.72	8.38
	t <sub>pF</sub>	3.61	2.60	1.30	2.50
	Avg <sub>pF</sub>	6.10	7.72	2.51	5.44
	Z <sub>pR</sub>	1.33	3.40	4.60	3.11
	t <sub>pR</sub>	0.89	1.85	0.57	1.10
	Avg <sub>pR</sub>	1.11	2.62	2.58	2.11
	Avg <sub>p</sub>	3.60	5.17	2.55	<b>3.77</b>
	z <sub>s</sub>	3.26	10.13	4.60	6.00
	t <sub>s</sub>	1.63	0.12	1.83	1.19
	Avg <sub>s</sub>	2.44	5.12	3.22	<b>3.59</b>
	Avg <sub>tot</sub>	3.22	5.16	2.77	<b><u>3.71</u></b>
EFD-MBD	z <sub>s</sub>	16.40	0.54	16.68	11.21
	t <sub>s</sub>	2.95	13.22	2.90	6.35
	Avg <sub>s</sub>	9.67	6.88	9.79	<b>8.78</b>
CFD-MBD-1- Way	Z <sub>pF</sub>	14.54	53.97	40.98	36.50
	t <sub>pF</sub>	6.71	3.53	5.39	5.21
	Avg <sub>pF</sub>	10.62	28.75	23.19	20.85
	Z <sub>pR</sub>	17.45	19.85	15.63	17.64
	t <sub>pR</sub>	4.58	7.59	5.09	5.75
	Avg <sub>pR</sub>	11.01	13.72	10.36	11.70
	Avg <sub>p</sub>	10.82	21.23	16.77	<b>16.28</b>
	z <sub>s</sub>	12.04	7.41	15.94	11.79
	t <sub>s</sub>	3.92	13.06	10.54	9.18
	Avg <sub>s</sub>	7.98	10.23	13.24	<b>10.48</b>
	Avg <sub>tot</sub>	9.87	17.57	15.60	<b><u>14.35</u></b>
CFD-MBD-2- Way	Z <sub>pF</sub>	25.33	0.46	53.04	26.28
	t <sub>pF</sub>	4.53	3.43	8.14	5.37
	Avg <sub>pF</sub>	14.93	1.94	30.59	15.82
	Z <sub>pR</sub>	14.38	42.66	18.06	25.04
	t <sub>pR</sub>	0.86	6.38	4.36	3.87
	Avg <sub>pR</sub>	7.62	24.52	11.21	14.45
	Avg <sub>p</sub>	11.28	13.23	20.90	<b>15.14</b>
	z <sub>s</sub>	28.12	17.03	49.35	31.50
	t <sub>s</sub>	7.66	9.55	12.77	9.99
	Avg <sub>s</sub>	17.89	13.29	31.06	<b>20.75</b>
	Avg <sub>tot</sub>	13.48	13.25	24.29	<b><u>17.01</u></b>
Diff (E <sub>1Way</sub> -E <sub>2Way</sub> )	Avg <sub>pF</sub>	-4.31	26.81	-7.40	5.03
	Avg <sub>pR</sub>	3.39	-10.81	-0.85	-2.75
	Avg <sub>p</sub>	-0.46	8.00	-4.13	1.14
	Avg <sub>s</sub>	-9.91	-3.06	-17.82	-10.26
	Avg <sub>tot</sub>	-3.61	4.31	-8.69	-2.66

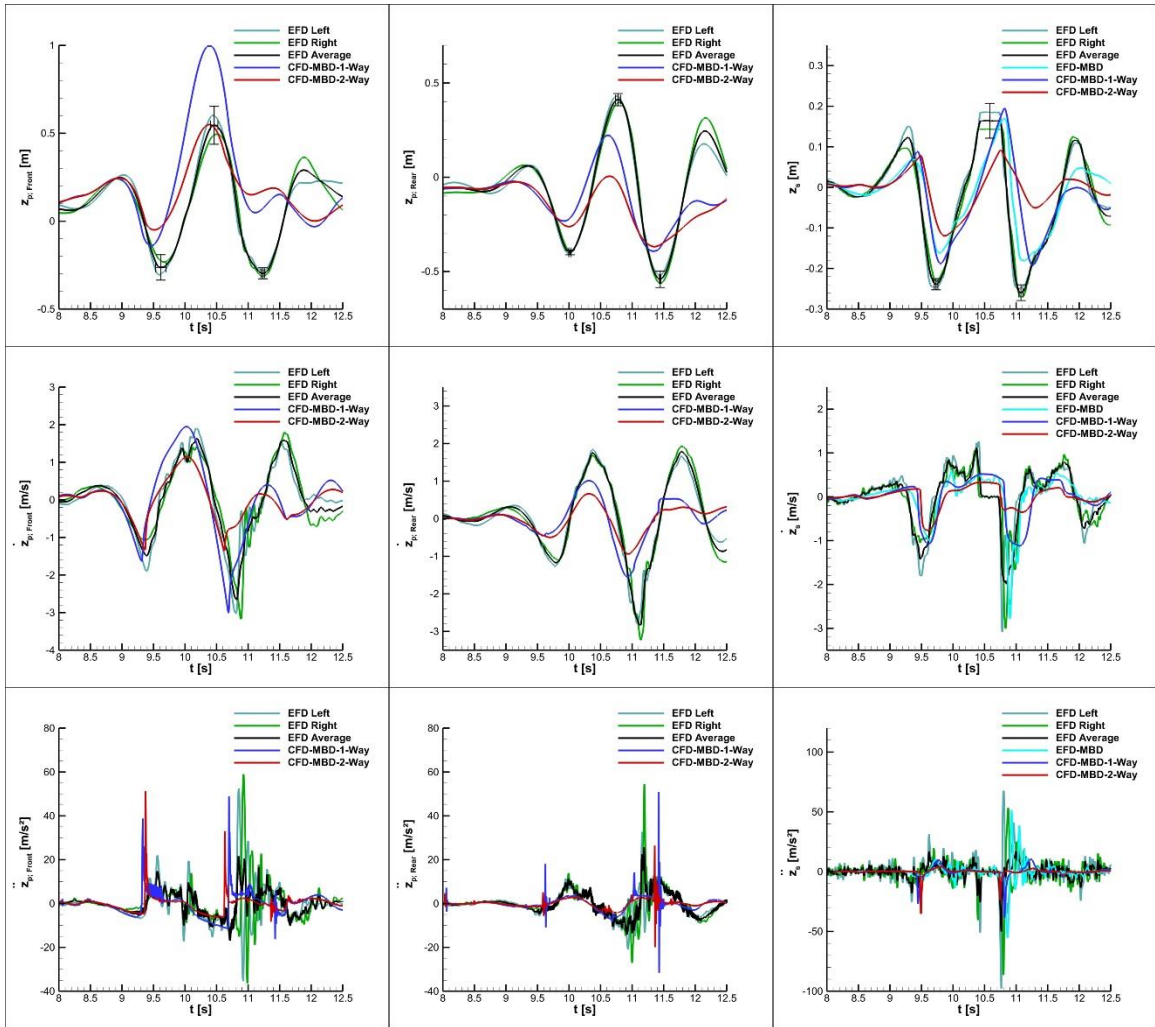


Figure 7-5 WAM-V single-wave simulation results

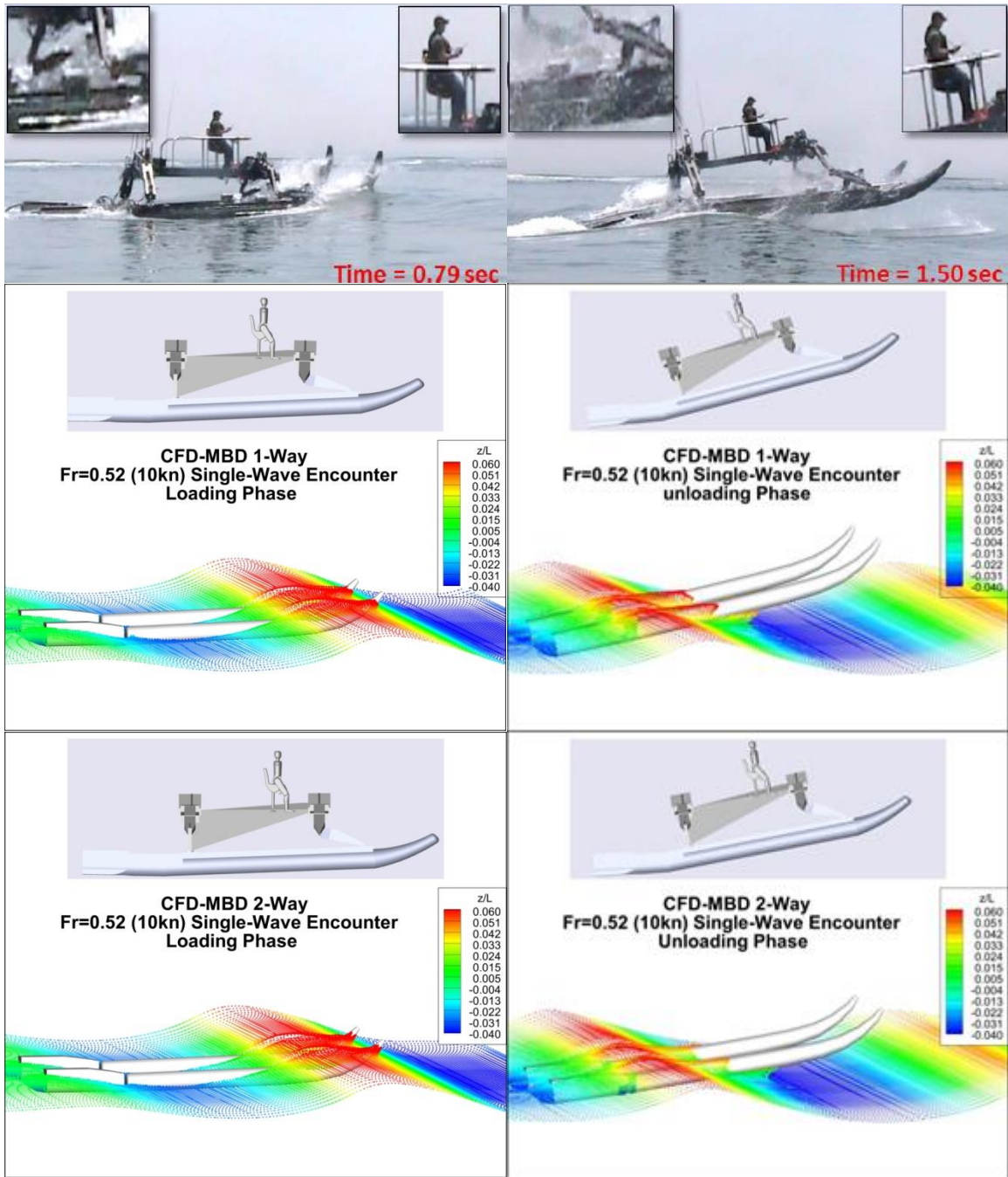


Figure 7-6 Snapshots of experimental videos and CFD-MBD simulations during single-wave event

## 7.4 WAM-V Rough Water

Rough-water validation results are shown in Table 7-4. EFD acceleration data show asymmetry with 10.8% difference between right and left pontoons for the front and 8.4% for the rear posts, with an average of 9.6%. The CFD-MBD average error values for pontoon accelerations are 38% for 1-way and 25%D for 2-way. For suspension accelerations, the average error values are 39% for 1-way and 20%D for 2-way. This is consistent with 2DoF cylinder drop in that error values for 2-way simulation are smaller for suspension than pontoon. Compared to 1-way, error values are reduced by 13%D for pontoon and 19% for suspension, with an average of 15%. This is again consistent with 2DoF cylinder drop in that 2-way coupling reduces the error values for suspension more significantly than pontoon. The overall average error values are 38% for 1-way and 24%D for 2-way. The agreement with EFD is reasonable, as shown in Figure 7-7, given that a regular head wave representation of the asymmetric irregular seas is used in simulations.

CFD-MBD 1-way and 2-way simulations are compared in Figure 7-8. For heave motions, 2-way coupling induces a phase lag, while heave amplitudes are similar. For pitch motions, 2-way coupling reduces the amplitude by 35%. For engine pod angle, the 2-way coupling induces a downward pod effect, being 2.2 degrees for the peak values. For total resistance coefficient, 2-way coupling reduces the amplitude by 37%. For relative suspension motion, 2-way coupling reduces the amplitude by 48%. Figure 7-9 shows free-surface and WAM-V motions at four increments during the last encounter period simulated, where some of the differences between 1-way and 2-way results are visually evident.

**Table 7-4 WAM-V rough-water sea-trials and CFD-MBD validation simulations in regular waves representation of the irregular seas**

Acceleration		EFD (Irregular Waves)			CFD (Regular Waves, $\lambda/L=1.33$ )								
					Values		E% D <sub>Left</sub>		E% D <sub>Right</sub>		E <sub>Avg</sub>		
		Left	Right	Diff (%)	1-way	2-way	1-way	2-way	1-way	2-way	1-way	2-way	Diff. (E <sub>1way</sub> -E <sub>2way</sub> )
Pontoon Front	EV (G's)	-0.012	-0.0011	-	-0.049	0.012	-	-	-	-	-	-	-
	SD (G's)	0.47	0.63	29.09	0.48	0.40	2.13	14.89	23.81	36.51	12.97	25.70	-12.73
	Dom Freq (Hz)	0.733	0.733	0.00	0.726	0.726	0.93	0.93	0.93	0.93	0.93	0.93	0.00
	Dom Amp (G's)	0.287	0.297	3.42	0.628	0.496	118.97	73.05	111.31	66.99	115.14	70.02	45.12
	Avg			10.84			40.68	29.63	45.35	34.81	<b>43.01</b>	<b>32.22</b>	<b>10.79</b>
Pontoon Rear	EV (G's)	0.004	-0.0011	-	-0.013	-0.0082	-	-	-	-	-	-	-
	SD (G's)	0.35	0.32	8.96	0.12	0.19	65.71	45.71	62.50	40.63	64.11	43.17	20.94
	Dom Freq (Hz)	0.733	0.733	0.00	0.726	0.726	0.93	0.93	0.93	0.93	0.93	0.93	0.00
	Dom Amp (G's)	0.24	0.20	18.18	0.15	0.23	40.01	4.49	27.52	15.40	33.76	9.94	23.82
	Avg			8.43			35.55	17.05	30.32	18.99	<b>32.93</b>	<b>18.02</b>	<b>14.92</b>
Pontoon Average	Avg			9.64			38.12	23.34	37.84	26.90	<b>37.97</b>	<b>25.12</b>	<b>12.85</b>
Susp	EV (G's)				-0.0006	-0.0070					-	-	-
	SD (G's)				0.4508	0.3021					10.34	26.06	-15.72
	Dom Freq (Hz)				0.726	0.726					0.86	0.86	0.00
	Dom Amp (G's)				0.665	0.432					106.15	33.96	72.19
	Avg										<b>39.11</b>	<b>20.29</b>	<b>18.82</b>
Avg	SD (G's)										29.14	31.64	-2.50
	Dom Freq (Hz)										0.91	0.91	0.00
	Dom Amp (G's)										85.02	37.97	47.04
	Avg										<b>38.35</b>	<b>23.51</b>	<b>14.85</b>

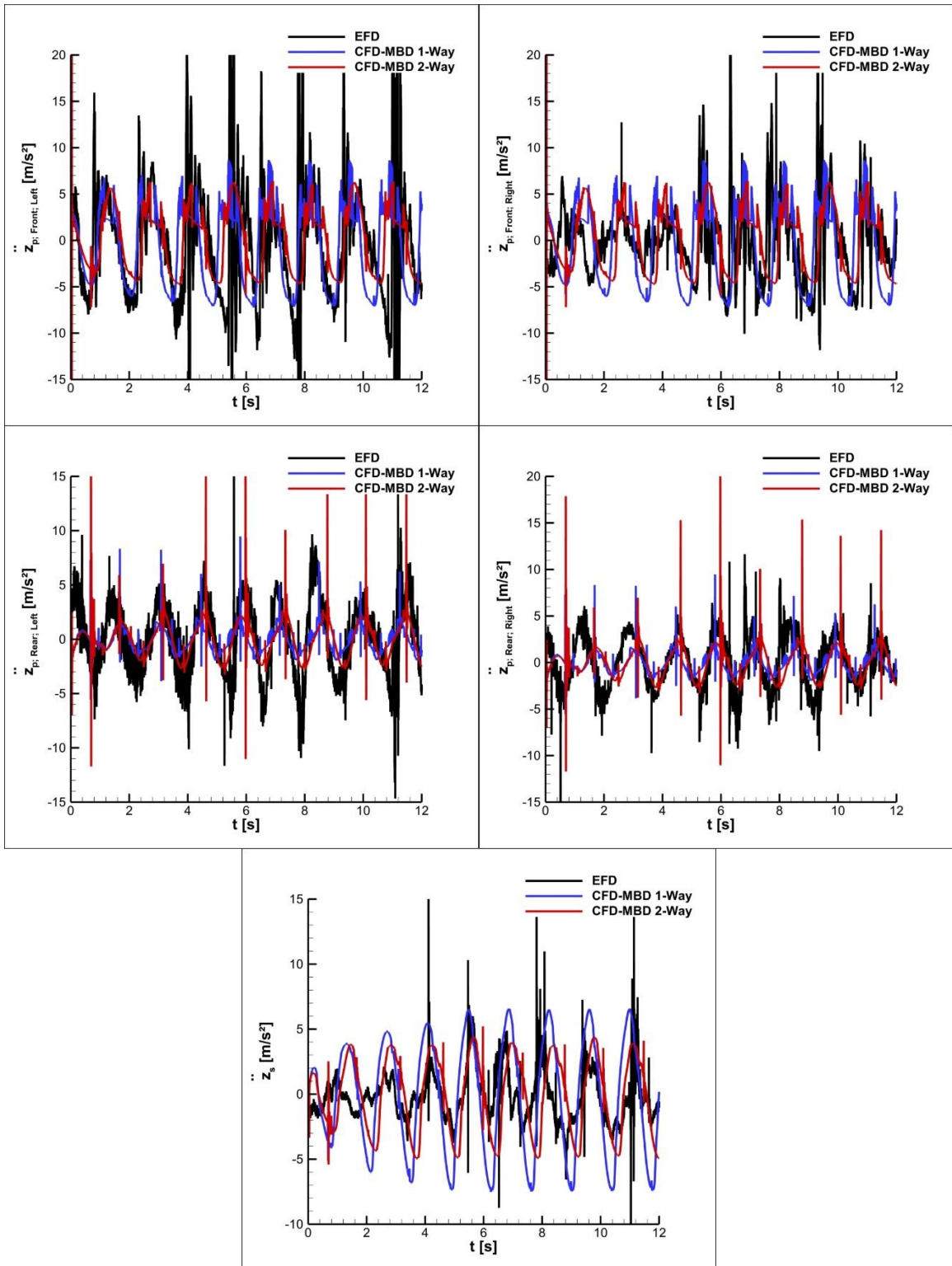


**Figure 7-7 WAM-V rough-water validation results against acceleration data**



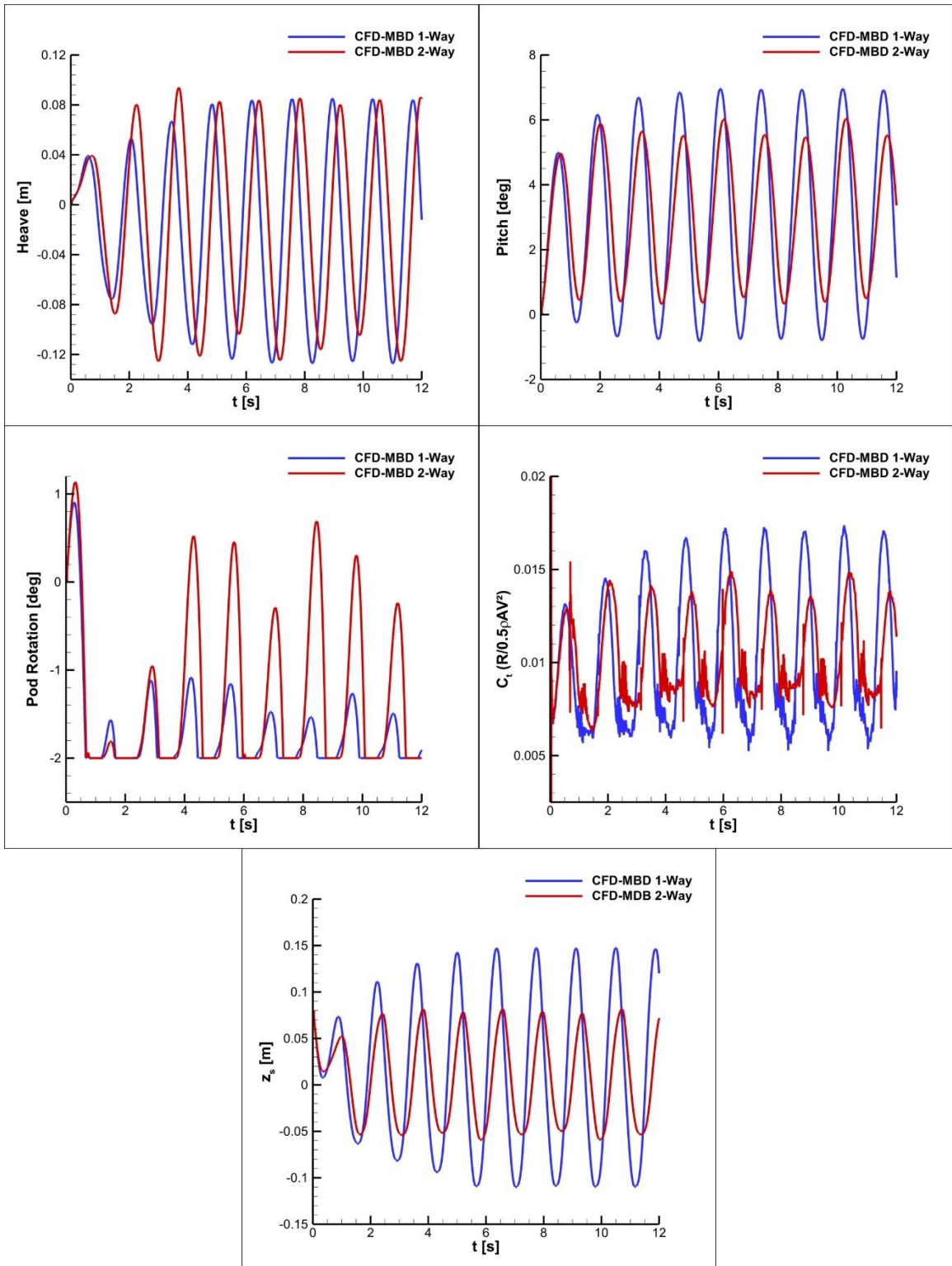


**Figure 7-8 Comparison of CFD-MBD 1-way and 2-way simulations in regular waves**

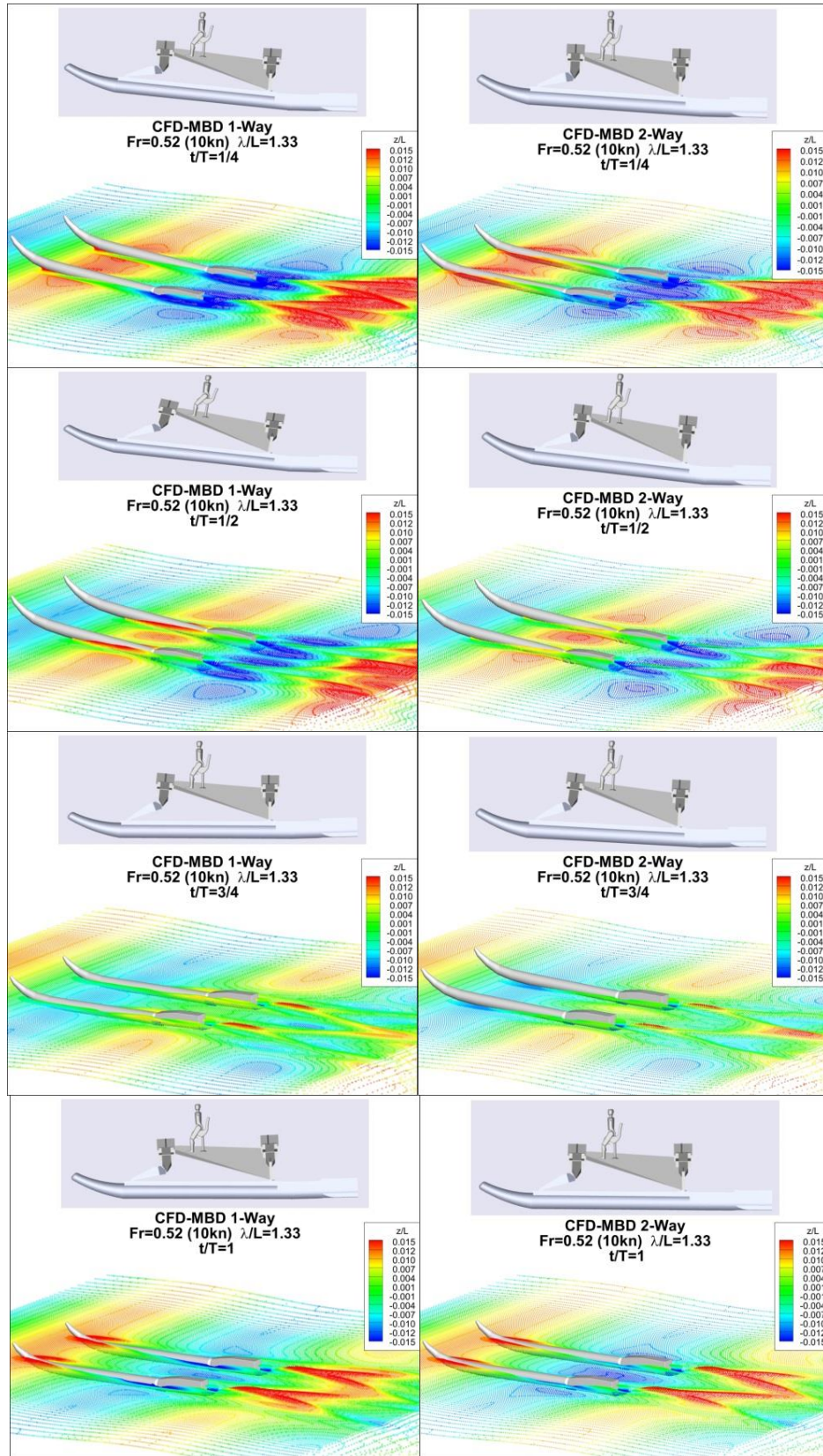


Figure 7-9 Free-surface and WAM-V motions for simulations in regular waves

## CHAPTER 8 CONCLUSION AND FUTURE WORK

CFD-MBD FSI is developed and validated by full-scale experiments for a novel hull form, WAM-V. CFDShip-Iowa is used as CFD solver, and is coupled to Matlab Simulink MBD models for cylinder drop and WAM-V. The flexible pontoons are modeled as rigid body.

FSI validation experiments are carried out, including cylinder drop with suspended mass and 33 ft WAM-V sea-trials with suspended payload. Data is collected for pontoon and suspension motions.

For 1DOF cylinder drop, CFD V&V studies are carried out including grid and time-step verification studies. CFD simulations with fine grid and medium time-step are validated with an overall average error of 7.6%DR. For the previously developed non-physics-based SB model [16], the overall average error is 2.8%DR.

For 2DOF cylinder drop, the overall average error for EFD-MBD (un-coupled MBD) is 7.7%DR. For CFD-MBD, the overall average error decreases by 10.6%DR for 2-way coupling compared to 1-way. Examination of pontoon and suspension displacement results show that some of the important physical features of the 2DOF drop are completely missed in 1-way simulations. For 2-way coupling, the average error is  $E=7.6\%DR$  for pontoon, same value as CFD 1DOF,  $E=3.7\%DR$  for suspension, with an overall average error value of  $E=5.6\%DR$ . For SB-MBD, the overall average error was  $E=5.5\%DR$ .

For WAM-V in calm water, relative pod angle is validated with  $E=27.9\%DR$  for 1-way and 14.2%DR for 2-way, with  $U_D$  being 6.8%DR. The 13.2%DR error reduction for 2-way compared to 1-way is consistent with 2DOF cylinder drop, which showed 10.6%DR reduction. The induced effects by 2-way coupling compared to 1-way include slight rise-

up for sinkage, bow-down for trim, downward rotation for pod angle, and downward motion for suspension displacement. For 2-way coupling, the maximum trim angle is predicted to be 1.4 degrees bow up at  $Fr=0.52$ . The maximum upward pod angle is about 1.5 degrees at  $Fr=0.27$ , while the maximum downward angle is about 2.9 degrees at  $Fr=1.04$ .

For simulation of WAM-V in single-wave, incoming waves are approximated using visual estimates and experimental data for pontoon motions. The CFD-MBD pontoon and suspension error values are reduced by 1.1%DR and increased by 10.3%, respectively, compared to 1-way. Examinations of the results show that 2-way coupling significantly improves the prediction of the peak amplitude in pontoon motions for the front post location, while the extrema amplitudes for pontoon displacement at the rear post location and suspension motions are under-predicted. The same under-prediction is observed in EFD-MBD (un-coupled MBD), with an overall average error value of about 9%DR. The current 2-way results are validated with an overall average error value of 17%DR.

For WAM-V in rough-water, the experimental data are about 10% different between the right and left pontoons. However, symmetric conditions are assumed in simulations. The irregular seas are approximated by a representative regular wave with a frequency same as the dominant frequency in EFD data and an  $H/\lambda$  of  $1/64$ , the typical value for sea-state 3. CFD-MBD error values for 2-way coupling are reduced by 13%D for pontoon and 19% for suspension compared to 1-way, consistent with 2DOF cylinder drop in that the error reduction is more significant for suspension. The induced effects by 2-way coupling compared to 1-way include a phase lag for heave, a reduction in pitch amplitude by 35%, a downward pod effect increasing the peak values by 2.2 degrees, a reduction in

total resistance amplitude by 37%, and a reduction in relative suspension motion amplitude by 48%. CFD-MBD 2-way coupling error values are 25%D for pontoon and 20%D for suspension, consistent with 2DOF cylinder drop in that the error is smaller for suspension. The overall average error value is 24%D for 2-way, which is reasonable given the differences between simulation waves and experiments.

Future work will need to include bi-linear or non-linear damping modeling for cylinder drop to simulate friction in the guide rails. A stiffness model needs to be implemented for WAM-V to simulate the compression bump stop for hinged pod. Single-wave simulations will be improved by further refining the incoming wave approximation and performing free-running simulations to predict the reduction in vessel speed. Modeling for flexible pontoons will need to be incorporated by coupling the current CFD-MBD with a finite element (FE) solver building on previous research using CFDSHIP-Iowa. Improved tow tank and/or wave basin experiments for captive and free-running conditions and full-scale sea-trials are needed for validation studies, including measurements for hull and suspension motions and pontoon flexibility. Validation studies for resistance and propulsion, sea-keeping, course keeping, and maneuvering will need to be carried out in calm water and regular and irregular seas for deep and shallow conditions using propulsion models and real propulsor simulations.

## REFERENCES

- [1] Bautista JQ, Riley MR, Kuehne HL, and Irvine MJ (2009) Marine Advanced Research WAM-V Proteus Propulsion, Seakeeping, and Miscellaneous Trials. Report NSWCCD-23-TM-2009/43, Naval Surface Warfare Center Carderock Division, West Bethesda, Maryland, July.
- [2] Conger M, Mousaviraad SM, Stern F, Peterson A, Ahmadian M (2014) URANS CFD for Two-Body Hydrodynamic Simulation of Wave Adaptive Modular Vessels (WAM-V) and Validation against Sea Trials. *Naval Engineers Journal*, 126(4): 47–52.
- [3] Conti U and Gundersen M (2011) Second Generation Design of Wave Adaptive Modular Vessels (WAM-V®): A Technical Discussion of Design Improvements. *Proceedings of 11th International Conference on Fast Sea Transportation*, Honolulu, Hawaii, USA, September 2011, pp.772-776.
- [4] Ding F, Han X, Zhang N, and Luo Z (2014) Characteristic analysis of pitch-resistant hydraulically interconnected suspensions for two-axle vehicles. *Journal of Vibration and Control*. Epub ahead of print 20 March 2014. DOI: 10.1177/1077546314520829.
- [5] ElMadany MM and Qarmoush AO (2011) Dynamic Analysis of a Slow-active Suspension System Based on a Full Car Model. *Journal of Vibration and Control* 17(1): 39-53.

- [6] Fratello J and Ahmadian M (2011) Multi-body Dynamic Simulation and Analysis of Wave-adaptive Modular Vessels. In: Proceedings of 11th International Conference on Fast Sea Transportation, Honolulu, Hawaii, USA, September 2011, pp.777-783.
- [7] Helsel KJ, Pollara AS, and Rod DA (2011) WAM-V (Proteus) Prototype Model Testing. Naval Research Enterprise Intern Program Final Report, Sumer 2011.
- [8] Huang J, Carrica P, Stern F (2008) Semi-coupled air/water immersed boundary approach for curvilinear dynamic overset grids with application to ship hydrodynamics. *International Journal Numerical Methods Fluids* 58: 591-624.
- [9] Jayachandran R and Krishnapillai S (2012) Modeling and optimization of passive and semi-active suspension systems for passenger cars to improve ride comfort and isolate engine vibration. *Journal of Vibration and Control* 19(10): 1471-1479.
- [10] Jeon SH, Cho YU, Seo MW, Cho JR, and Jeong WB (2013) Dynamic response of floating substructure of spar-type offshore wind turbine with catenary mooring cables. *Ocean Engineering* 72: 356-364.
- [11] Mousaviraad SM, Carrica PM, Stern F (2010) Development and Validation of Harmonic Wave Group Single-Run Procedure for RAO with Comparison to Regular Wave and Transient Wave Group Procedures Using URANS. *Journal of Ocean Engineering* 37: 653-666.
- [12] Mousaviraad SM, Bhushan S, and Stern F (2013) URANS Studies of WAM-V Multi-Body Dynamics in Calm Water and Waves. In: Third International Conference on Ship Maneuvering in Shallow and Confined Water, Ghent, Belgium.

- [13] Nassif HN and Liu M (2004) Analytical Modeling of Bridge-Road-Vehicle Dynamic Interaction System. *Journal of Vibration and Control* 10(2): 215-241.
- [14] Nieto AJ, Morales, AL, Chicharro JM, and Pintado P (2014) An adaptive pneumatic suspension system for improving ride comfort and handling. *Journal of Vibration and Control*. Epub ahead of print 30 June 2014. DOI: 10.1177/1077546314539717.
- [15] Peterson AW and Ahmadian M (2011) Simulation and Testing of Wave-adaptive Modular Vessels. In: *Proceedings of 11th International Conference on Fast Sea Transportation*, Honolulu, Hawaii, USA, September 2011, pp.784-789.
- [16] Peterson AW (2013) *Simulation and Testing of Wave-Adaptive Modular Vessels*. Master's Thesis, Virginia Polytechnic Institute and State University, Blacksburg, Virginia.
- [17] Rudman M and Cleary PW (2013) Rogue wave impact on a tension leg platform: The effect of wave incidence angle and mooring line tension. *Ocean Engineering* 61: 123-138.
- [18] Soong MF, Ramli R, and Mahadi WNL (2015) Using gear mechanism in vehicle suspension as a method of altering suspension characteristic. *Journal of Vibration and Control* 21(11): 2187-2199.
- [19] Yang Z, Ramli R, and Mahadi WNL (2014) Vibration suppression of four degree-of-freedom nonlinear vehicle suspension model excited by the consecutive speed humps. *Journal of Vibration and Control*. Epub ahead of print 25 July 2014. DOI: 10.1177/1077546314543728.



- [20] Zambrano T, MacCready T, Kiceniuk T Jr, Roddier DG, and Cermelli CA (2006)  
Dynamic Modeling of Deepwater Offshore Wind Turbine Structures In Gulf of  
Mexico Storm Conditions. In: Proceedings of 25th International Conference on  
Offshore Mechanics and Arctic Engineering, Hamburg, Germany, 4-9 June 2006.